ChemElectroChem

Review
doi.org/10.1002/celc.202400705

Chemistry Europe
European Chemical Societies Publishing

www.chemelectrochem.org

Navigating the Challenges of Rechargeable Aluminum Battery Research: Material Instabilities, Technical Hurdles, and Future Directions

Eliana Fuentes-Mendoza, Mahla Talari, Eugen Zemlyanushin, Rafael Cordoba, Noha Sabi, and Sonia Dsoke*

Rechargeable aluminum (Al) batteries (RABs) are promising electrochemical energy storage systems due to their claimed high safety standards, low cost, and lightweight materials. However, their application is limited by the corrosivity of the chloroaluminate ionic liquid-based electrolyte, which is currently the only type of electrolyte able to plate and strip Al efficiently. Despite there are several recent reviews discussing progress in the field of Al batteries, it is believed that it is also necessary to consider the challenges and the many failures often not presented in publications, which are required to further develop the technology. This review examines the technical challenges in developing RAB technologies, based on the direct experience of research group, emphasizing the critical role of selecting appropriate electrolytes, passive components, and cell setups for understanding and correctly assessing electrode material performance. RABs are still in their infancy and to build a comprehensive bibliography, technical challenges should be thoroughly documented and addressed. The authors aim to provide practical guidelines to help researchers and newcomers in the RAB field avoid common pitfalls and overcome the challenges that impede achieving the theoretical advantages of RABs.

1. Introduction

Sustainable energy storage systems play a crucial role in achieving the goal of decarbonization set by the European Union for 2050.[1] Lithium-ion batteries (LIBs) are currently dominating the market, but are facing concerns in terms of cost and sustainability due to their reliance on critical raw materials and elements which are raising geopolitical concerns (such as Li, Co, and Ni). These are the main drivers pushing researchers to investigate novel battery chemistry alternatives to lithium. In the plethora of "post-LIBs chemistries", Na-ion batteries reached a certain maturity and started penetrating the market.[2] Divalent battery chemistries, including Zn-, Mg-, and Ca-based batteries, rely on the transport of two charges per exchanged cation, showing promising performance in terms of capacity, but each one of them presents particular challenges (e.g., dendrite formation and gas evolution with Zn-ion batteries, insulating/blocking passivation layer for Mg and Ca anodes, etc.).[3] Moving from a divalent to a trivalent cation would be very appealing due to the theoretical transfer of three charges per exchanged ion and here lies the interest in developing rechargeable Al-ion batteries (RABs).

RABs caused a great stir in the field of alternative and complementary energy storage systems. The following advantageous properties make Al metal a more attractive choice as a negative electrode for RABs in comparison with the metallic Li as an anode for LIBs: high safety standards because of its reduced reactivity in environments where lithium would react, low costs due to the high abundance of Al in the crust of the earth, lightweight material, and, in some specific cases like when graphite enables the intercalation of $AlCl_4^-$, RABs possess very fast charge and discharge processes.[4] While these positive aspects are often highlighted, they are accompanied by significant drawbacks. For instance, the use of chloroaluminate ionic liquid (IL)-based electrolytes introduces challenges such as high viscosity, low ionic conductivity at room temperature, sensitivity to moisture, and high corrosivity. These factors hinder the development of efficient and scalable rechargeable Al batteries (RABs).

Challenges and failures are important steps toward developing a successful technology, as evidenced several times in history (e.g., how many times did Edison fail before inventing the bulb?). However, often, failed experiments remain constrained in the

E. Fuentes-Mendoza, M. Talari, E. Zemlyanushin, R. Cordoba
Institute for Applied Materials (IAM)
Karlsruhe Institute of Technology (KIT)
Hermann-von-Helmholtz-Platz 1, 76344 Eggenstein-Leopoldshafen, Germany

N. Sabi
High Throughput Multidisciplinary Research (HTMR)
Mohammed VI Polytechnic University
Lot 660 Hay Moulay Rachid, Ben Guerir 43150, Morocco

S. Dsoke
Department of Electrical Energy Storage
Fraunhofer Institute for Solar Energy Systems
Heidenhofstr. 2, 79110 Freiburg, Germany
E-mail: sonia.dsoke@ise.fraunhofer.de

S. Dsoke
Freiburg Materials Research Center-FMF
University of Freiburg
Stefan-Meier Str. 21, 79104 Freiburg, Germany

S. Dsoke
Institute for Sustainable Systems Engineering (INATECH)
University of Freiburg
Emmy-Noether-Straße 2, 79110 Freiburg, Germany

respective research group and only successful experiments are published. With this review, we would like to share with the research community our experience in the journey of developing RABs, hoping that this could help other researchers advance this technology. The review is structured in two main parts: the first one is dedicated to the review of the current state of the different cell's components in RABs; the second part describes the main challenges reported in the literature and encountered by our group while exploring materials for RABs.

2. Electrolytes

RABs operate through reversible Al plating/stripping on the negative electrode during charging and discharging. In RABs, similarly to other metal–ion batteries, the electrolyte enables ion transport between the two electrodes and allows reversible Al plating at the negative electrode. The electrolyte in any battery type should be carefully selected, as it significantly influences key performance metrics such as capacity, cycling stability, coulombic efficiency, and overall safety.

Over the years, various electrolytes have been used to enable Al plating, with some applied in the Al electroplating research community for the formation of Al protective layers on other metals and others specifically developed for RABs. High-temperature chloroaluminate molten salts, composed of Al chlorides and alkali metal chlorides, have historically been used for Al plating at first with a focus on the formation of Al protective layers on other metals and later on adapted for RABs.[5–8] These binary or ternary mixtures lower the otherwise high melting points

Eliana Fuentes-Mendoza is currently a Ph.D. candidate under the supervision of Prof. Helmut Ehrenberg at the Institute of Applied Materials—Energy Storage Systems (IAM-ESS), Karlsruhe Institute of Technology (KIT). She holds a master's degree in chemical engineering and a second master's in materials science and engineering. She has co-authored a peer-reviewed article on solid oxide fuel cells and presented her work at academic conferences. Her research interests are advancing sustainable energy storage technologies through innovative material design and electrochemical engineering, specializing in the development of cathode materials and passive components for aluminum batteries.

Mahla Talari is a Ph.D. graduate from the Institute of Applied Materials—Energy Storage Systems (IAM-ESS), Karlsruhe Institute of Technology (KIT), where she specialized in electrolyte development for aluminum rechargeable batteries, with a focus on addressing corrosion issues related to their electrolytes. She holds a master's degree in corrosion and protection of materials. Mahla has authored a peer-reviewed article on the possibility of aluminum plating and stripping, as well as side reactions in noncorrosive electrolytes for aluminum rechargeable batteries. She has also presented her research at academic conferences. Her research interests center on advancing energy storage technologies and electrochemical engineering.

Eugen Zemlyanushin is currently a Ph.D. candidate under the supervision of Prof. Helmut Ehrenberg at the Institute of Applied Materials—Energy Storage Systems (IAM-ESS), Karlsruhe Institute of Technology (KIT). He obtained his B.Sc. degree in 2019 at the Institute of Organic Chemistry—Laboratory of Applied Chemistry, KIT. His electrochemical research started with the investigation of honeycomb-type structure of cathode materials for sodium-ion batteries (SIBs). He received his master's degree for his work on rechargeable aluminum batteries (RABs) in 2021. His research is focused on the negative electrode, current collector, and binder materials for RABs.

Rafael Cordoba studied chemistry at the University of Córdoba (Spain) and obtained a master's degree in Chemical Sciences and Technologies from the Complutense University of Madrid (Spain). He obtained his Ph.D. at the University of San Pablo-CEU (Spain) in 2022, focusing on vanadium compounds as cathodes for sodium-ion batteries. He currently holds a postdoctoral research position at the Karlsruhe Institute of Technology (Germany). His research is based on cathodes for rechargeable aluminum batteries.

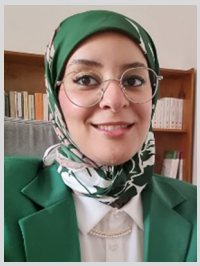

Noha Sabi received her master's degree in functional materials and Ph.D. in electrochemistry/materials for batteries from Cadi Ayyad University Marrakech, Morocco, in collaboration with Mohammed VI Polytechnic University Benguerir, Morocco. In 2019, she was a visiting scientist at the Pacific Northwest National Laboratory (PNNL), in Washington. She was a post-doctoral fellow researcher within the Materials Synthesis Group at the Karlsruhe Institute of Technology (KIT), Karlsruhe, Germany. She is currently an assistant professor at the High Throughput Multidisciplinary Research Laboratory (HTMR-Lab) at Mohammed VI Polytechnic University.

Sonia Dsoke is a professor at the University of Freiburg and leader of the group "Advanced Battery Materials" at Fraunhofer ISE. She obtained her Ph.D. in chemistry in 2005 at the University of Camerino (Italy). Sonia Dsoke contributed to leading institutions such as the Center for Solar Energy and Hydrogen Research (ZSW), the Karlsruhe Institute of Technology (KIT), and the Cluster of Excellence POLiS. Her main research subjects are related to developing functional materials for electrochemical energy storage systems, with a special focus on tackling the challenges of novel battery concepts such as Na, Zn, Al, and S-based batteries.

of individual components, enabling electrolyte operation at 100–200 °C. Early studies of $AlCl_3$KCl–NaCl,[8–10] followed by the development of $AlCl_3$–LiCl–KCl,[11] which exhibited a low melting point (95 °C) and high performance in Al/graphite batteries. However, despite promising electrochemical properties, challenges such as high operating temperatures and Al dendrite formation limited practical applications of high-temperature molten salts.[9,12] This led to the development of alternative electrolytes such as room-temperature ionic liquid-based electrolytes (RTILs).

Figure 1 presents a timeline illustrating the evolution of these electrolytes, showcasing the progress from high-temperature molten salts to polymer-based electrolytes. In the following sections, we examine the different categories of electrolytes commonly used in RABs to understand their unique properties and challenges.

2.1. RTILs

RTILs are attractive for RABs because they possess excellent properties like low flammability, negligible vapor pressure, relatively high ionic conductivity, a melting point of often below 100 °C, and wide electrochemical stability windows.[13–20]

A key innovation in RTIL development was the substitution of metal cations (like Na^+ or Ca^{2+}) in molten salts with long-chain organic cations.[21,22] This substitution decreases the melting point, resulting in RTILs that operate at ambient temperatures, offering practical simplicity.[23–26] The cation type in RTILs significantly impacts factors like viscosity, melting point, and ionic conductivity. Imidazolium cations (Im^+) with varying alkyl chains, such as 1-butyl-3-methylimidazolium ($BMIm^+$) and 1-ethyl-3-methylimidazolium ($EMIm^+$), are popular choices.[27,28] RABs primarily rely on chloride (Cl^-) associated with the cation due to its superior conductivity and stability compared to Br^- and I^-.[24] For example, at 30 °C $AlCl_3$/[BMIm]Cl IL has a higher conductivity (9.1 mS cm^{-1}) than $AlCl_3$/[BMIm]Br (8.6 mS cm^{-1}) and $AlCl_3$/[BMIm]I (4.3 mS cm^{-1}). Additionally, $AlCl_3$/[BMIm]Cl has a wider electrochemical stability window, ranging from −2.1 to 2.6 V versus Al ($\Delta E = 4.7$ V), compared to $AlCl_3$/[BMIm]Br which ranges from −1.9 to 2.0 V versus Al ($\Delta E = 3.9$ V), and $AlCl_3$/[BMIm]I which ranges from −2.0 to 1.0 V versus Al ($\Delta E = 2$ V). This has been related to the largest highest occupied molecular orbital-lowest unoccupied molecular orbital gap of $[BMIm]^+$–$[AlCl_4]^-$ ion pairs, which results in higher oxidation stability.[24]

Chloroaluminate ILs-based electrolytes, consisting of $AlCl_3$ and EMImCl, are among the most studied electrolytes for RABs.[29] In these electrolytes, Al plating is influenced by the molar ratio of $AlCl_3$:EMImCl and the equilibrium between various anionic species, as Al exists as Al-complexes rather than free Al^{3+}.[7,30]

In basic electrolytes ($AlCl_3$:EMImCl < 1), $AlCl_4^-$ and Cl^- are the predominant species, while neutral electrolytes ($AlCl_3$:EMImCl = 1) primarily contain $AlCl_4^-$; nonetheless, Al plating through $AlCl_4^-$, described in Equation (1), is an irreversible process and it requires high temperature to take place, leading to the reduction of organic $EMIm^+$ cation before $AlCl_4^-$ reduction.[31–33]

$$AlCl_4^- + 3e^- \rightarrow Al + 4Cl^- \quad (1)$$

For acidic electrolytes ($AlCl_3$:EMImCl > 1), $Al_2Cl_7^-$ becomes the dominant species alongside $AlCl_4^-$. $Al_2Cl_7^-$ is considered the "active" species for reversible Al plating and stripping through the reaction described in Equation (2).[31,34,35] Therefore, the capacity of the negative electrode comes essentially from the anolyte and it depends mainly on the availability of redox-active species, specifically $Al_2Cl_7^-$. The Al metal electrode serves only as a substrate for the Al plating and stripping processes.

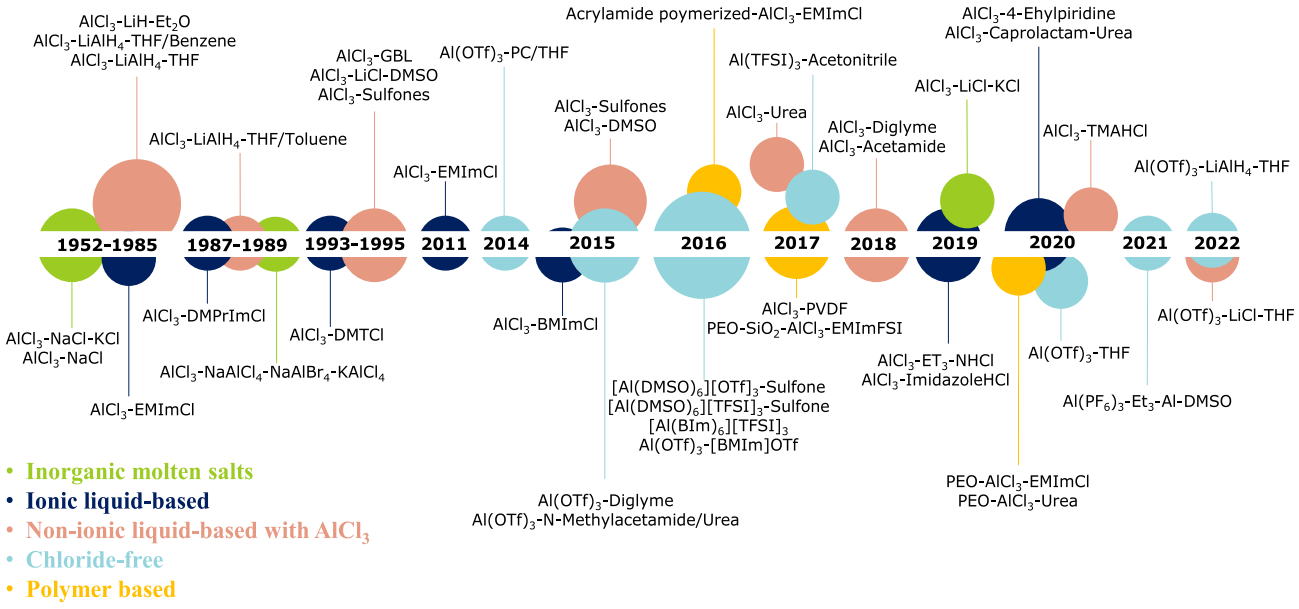

Figure 1. Timeline illustrating the development of electrolytes, highlighting the progression from high-temperature molten salts to polymer-based electrolytes.

$$4Al_2Cl_7^- + 3e^- \rightleftharpoons Al + 7AlCl_4^- \quad (2)$$

Increasing the acidity of the electrolyte has several advantages: 1) it facilitates the activation of Al plating by removing the native surface oxide (Al_2O_3) present on the surface of Al metal and, 2) it increases the RAB's energy density due to the higher amount of electrochemically active species; for instance, increasing the $AlCl_3$:EMImCl molar ratio from 1.3 to 2 can increase the energy density from 33 to 62 Wh kg^{-1} and decrease the average operating voltage from 2 to 1.4 V.[36] However, its acidic nature makes it highly corrosive. This corrosivity poses safety risks and limits compatible materials for current collectors and other battery cell components including coin cell cases.[23,37–39]

Moreover, the volume of the electrolyte in RABs is crucial. As stated earlier, electrolyte species, particularly $Al_2Cl_7^-$, are essential for the reversible Al plating/stripping at the negative electrode. Ensuring enough amount of electrolyte is essential not only for maintaining the energy density but also for sustaining long-term cycling stability, as electrolyte consumption can degrade the cell's performance over time. Therefore, the performance of the negative electrode and the entire RAB is linked to the electrolyte's volume and molar ratio (i.e., quantity of $Al_2Cl_7^-$ species).

2.2. Electrolytes Based on $AlCl_3$ and Organic Solvents

$AlCl_3$ in organic solvents was studied to potentially decrease the corrosivity of the electrolyte. Various solvents like propylene carbonate (PC), tetrahydrofuran (THF), acetonitrile (ACN), and γ-butyrolactone (GBL) were investigated and the results obtained by using these electrolytes for Al plating and stripping are summarized in **Table 1**. However, some of these studies did not explore the possibility of reversible Al plating/stripping, as they were not oriented toward battery research.

The main limitation of these studies was the low concentration of $AlCl_3$ (around 1 M), which was insufficient to promote the formation of the acidic Lewis anion $Al_2Cl_7^-$. Instead, it primarily led to the formation of $AlCl_4^-$ and $[AlCl_2(solvent)_n]^+$. Increasing the $AlCl_3$ concentration to a critical point (often a 1:1 molar ratio with the solvent), resulting in "solvate ionic liquids" with properties similar to ILs.[40,41] In brief, it seems that investigation of $AlCl_3$ in organic solvents holds potential for improving electrolyte performance in terms of reversible Al plating/stripping. Recently, it has been reported that locally concentrated IL electrolytes formed via diluting the IL with nonsolvating solvents such as 1,2-difluorobenzene does not affect the $Al_2Cl_4^-/Al_2Cl_7^-$ equilibrium, thus preserving the plating and stripping ability.[42]

Early studies have explored $AlCl_3$ combined with metal hydrides like lithium hydride (LiH) or lithium aluminum hydride ($LiAlH_4$) in organic solvents for industrial-scale Al plating. Initial investigations used $AlCl_3$ and LiH in diethyl ether (Et_2O), achieving Al plating.[5] Subsequent studies focused on less volatile solvents like THF, exploring various additives and solvent combinations, which are summarized in Table 1. The results of these studies suggest that higher $LiAlH_4$:$AlCl_3$ ratios enhance Al plating by promoting the hydride-facilitated charge transfer process (H^-).[43–46]

The primary similarity between RTILs and electrolytes based on $AlCl_3$ and organic solvents is that reversible Al plating in both systems is enabled by the formation of Lewis acidic species. In RTIL-based electrolytes, this occurs when the $AlCl_3$:EMImCl molar ratio exceeds unity, resulting in the formation of the $Al_2Cl_7^-$ species. Similarly, in organic solvent-based systems, increasing the concentration of $AlCl_3$ promotes the generation of analogous Lewis acidic species, thereby mimicking the behavior observed in RTILs. For instance, in an $AlCl_3$:GBL system at a 1.5:1 ratio—comparable to that in $AlCl_3$:EMImCl—the formation of $[Al_3Cl_{10}]^-$ (a different species than that formed in $AlCl_3$:EMImCl system) enables Al plating, although stripping neither studied nor achieved within the tested potential window. While the text does not explicitly indicate whether GBL is detrimental to the system, maintaining the proper molar ratio of $AlCl_3$ to GBL is crucial for achieving optimal performance.[47]

Additionally, existing research lacks quantitative data on the corrosivity of these electrolytes compared to chloroaluminate IL-based electrolytes.[5–7,43–46,48–53] Developing chloride-free systems that address these limitations is crucial for practical RABs.

2.3. Chloride-Free Electrolytes

Since the acidity of the electrolyte is mainly determined by the presence of $AlCl_3$, developing chloride-free electrolytes for RABs may be the path to reduce the corrosivity issues. However, this path presents challenges such as the limited availability of commercial battery-grade Al salts with weakly coordinating anions.[54] The readily available options like aluminum trifluoromethanesulfonate ($Al(OTf)_3$) raise concerns about their effectiveness in dissociating within the electrolyte and the difficulty of proper drying. The residual water can potentially hinder Al cation solubility and activity and give rise to side reactions as it is discussed in the literature[12,55] and depicted in **Figure 2**. Additionally, the stability of the anion during Al plating/stripping is critical; for example, the decomposition of fluoride-containing anions can lead to the generation of insulating surface compounds that impede the reversible Al plating/stripping process.[56] Consequently, identifying a stable and weakly coordinating anion for the Al salt remains a significant hurdle in developing high-performance, chloride-free organic electrolytes for RABs.

While promising chloride-free electrolytes have been proposed, further research is needed to achieve balance among effective and Al plating/stripping, electrolyte stability, and corrosivity mitigation. The outcomes of several approaches using both synthesized Al salts and commercially available $Al(OTf)_3$ as an alternative to $AlCl_3$ are reviewed and summarized in Table 1.

3. Aluminum (Al) Negative Electrode

Common household Al with a purity of ≈99% is generally considered a cost-effective metal.[55] However, high-purity Al-foils are required to avoid side reactions of impurities such as iron (Fe) or chromium (Cr). In 2024, the price per kilogram (kg) of high-purity Al varied based on the level of purity: 4 N (99.99%) costs 261.95€ kg^{-1}, 5 N (99.999%) costs 475.95€ kg^{-1}, and 6 N (99.9999%) costs 950.95€ kg^{-1}. The production of primary

Table 1. Summary of research on Al plating in various electrolytes using synthesized or commercially available Al salts combined with different solvents.

Al salt	Additive	Solvent	Plating[a)]	Stripping[a)]	Remarks	References
$AlCl_3$	–	DMSO			Al was plated onto magnesium (Mg) at a high temperature of 110 °C. The resulting Al film exhibited poor adhesion.	[48]
$AlCl_3$	LiCl	DMSO			Al was plated on tungsten (W) using a molar ratio of $AlCl_3$:LiCl (2:1).	[49]
$AlCl_3$	–	Dialkylsulfone			While increasing $AlCl_3$ concentration in sulfone solvents facilitated $Al_2Cl_7^-$ formation and room-temperature Al plating. Concerns about corrosivity and low anodic stability remained.	[50,51]
$AlCl_3$	–	Diglyme (G_2)			The cationic active species $[AlCl_2(G_2)_2]^+$ formed, allowing Al plating, and potentially offering reduced corrosivity.	[52]
$AlCl_3$	–	Triglyme (G_3)			Al plating was not observed with G_3, possibly due to stronger interactions between Al-cations and the solvent.	[52]
$AlCl_3$	–	Tetraglyme (G_4)			Al plating was not achieved with G_4, possibly due to stronger Al-cation interactions with the solvent.	[52]
$AlCl_3$	–	Acetamide			Al was plated on W and copper (Cu) using an eutectic electrolyte with a molar ratio of $AlCl_3$ to acetamide of 1.1:1.5.	[53]
$AlCl_3$	–	GBL			$AlCl_3$:GBL (1.5:1 molar ratio) yielded electrochemically active $Al_3Cl_{10}^-$ anions and enabled Al plating, but Al stripping was not observed.	[47]
$AlCl_3$	LiH	Diethyl ether (Et_2O)			Successful Al plating was achieved in these electrolytes but the solvent was volatile.	[5]
$AlCl_3$	$LiAlH_4$	THF/Benzene			The mixture of THF with benzene increases the current densities for Al plating.	[6]
$AlCl_3$	$LiAlH_4$	THF/Toluene			THF mixtures with toluene increased Al plating current densities.	[7]
$AlCl_3$	$LiAlH_4$	THF			Possible Al plating. THF is a less volatile alternative to Et_2O.	[43–46]
$AlCl_3$	1,2-difluorobenzene				The presence of 1,2-difluorobenzene (dFBn) in the electrolyte promoted better kinetics for aluminum stripping and plating, leading to reduced polarization and improved rate capability.	[34]
$[Al(DMSO)_6][OTf]_3$	–	Sulfone			Cationic Al complexes with ligands have been explored. No plating was observed.	[54]
$[Al(DMSO)_6][TFSI]_3$	–	Sulfone			Cationic Al complexes with ligands result in no plating of Al.	[54]
$[Al(BIm)_6][TFSI]_3$	–	–			The low-melting complex exhibited both cathodic and anodic currents but with poor cycling efficiency due to electrolyte decomposition.	[54]
$Al(TFSI)_3$	–	AN			The large size of $TFSI^-$ promotes better Al salt dissociation. Al plating was achieved on Mo, but high overpotential was needed due to the presence of Al_2O_3.	[158]
$Al(PF_6)_3$		DMSO			Al plating/stripping was observed on Cu, however, formation of Al_2O_3 occurred during the initial stages due to DMSO decomposition.	[159]
$Al(PF_6)_3$	Et_3Al	DMSO			Introducing Et_3Al as a water scavenger mitigated the issue with the formation of AlF_3 due to traces of water	[159]
$Al(OTf)_3$	–	PC/ THF			No electrochemical activity of Al ions was observed via CV, suggesting the unsuitability of this combination for Al plating.	[12]
$Al(OTf)_3$		THF			Al plating near 0 V vs. Al was observed on Au, suggesting the formation of $Al(THF)_4^{3+}$ complexes. But the absence of a strong Lewis base limited Al stripping.	[160]
$Al(OTf)_3$	LiCl	THF			Adding LiCl to the electrolyte, enhanced Al ion activity, but Al stripping remained elusive even with a 1:3 ratio of $Al(OTf)_3$:LiCl.	[161]
$Al(OTf)_3$	$LiAlH_4$	THF			Al plating through the reduction of Al-hydride species on Cu and Au was confirmed using SEM and XPS, showing the crucial role of H^- in facilitating reversible Al plating/stripping.	[162]
$Al(OTf)_3$	–	G_2			$Al(OTf)_3$ complex with G_2 confirmed by FT-IR in concentration higher than 0.04 M, but no Al plating via CV was observed possibly due to chelation and electrode passivation by the electrolyte.	[153,154]
$Al(OTf)_3$	urea	NMA			Al complexes like $[AlOTf–solvent_x\text{-}urea_2]^{2+}$ formed in this electrolyte using 0.05 M of $Al(OTf)_3$. High ionic conductivity of 2.5 mS cm^{-1} at 30 °C and the wide electrochemical window of 3.5 V on Pt, but Al plating is not confirmed.	[148,155]

[a)]Green indicates confirmed Al plating and/or stripping, orange signifies no observed Al plating and/or stripping, and grey shows that the study did not explicitly evaluate Al plating and stripping using characterization techniques like SEM and XPS.

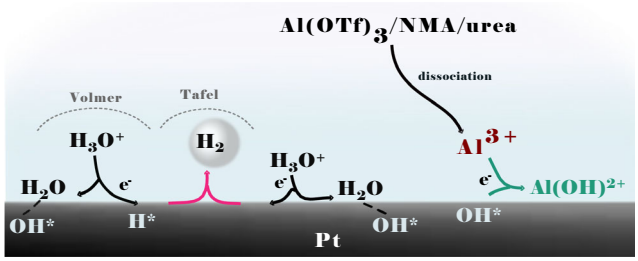

Figure 2. Illustration of the mechanism associated with the residual water from aluminum trifluoromethanesulfonate ($Al(OTf)_3$) salts which hinders Al plating.[51]

Al involves two main steps. First, alumina is extracted from bauxite through the Bayer process. Next, Al manufacturing occurs via the Hall–Héroult process to achieve a purity of 3 N (99.9%). Additional time and energy-intensive steps, such as vacuum distillation, three-layer electrolysis, and segregation, are necessary to achieve high or ultra-high-purity Al.[57,58] As aluminum purity increases, energy requirements rise, resulting in higher production costs.[59,60] An example for the energy consumption of different stages of Al production is visualized in **Figure 3**.

The Al industry contributes ≈1% of greenhouse gas emissions. Direct emissions (40%) result from the production process, while indirect emissions (60%) stem from high electricity demand.[61,62] Moreover, the highly alkaline red mud waste, a mix of iron (III)-hydroxide ($Fe(OH)_3$, iron (III)-oxide (Fe_2O_3), and sodium hydroxide (NaOH) solution, generated during Al production poses environmental and health risks. Soil and surface water pollution can occur near Al factories due to accidents, weathering, and water erosion as was observed in Hungary in October 2010.[57]

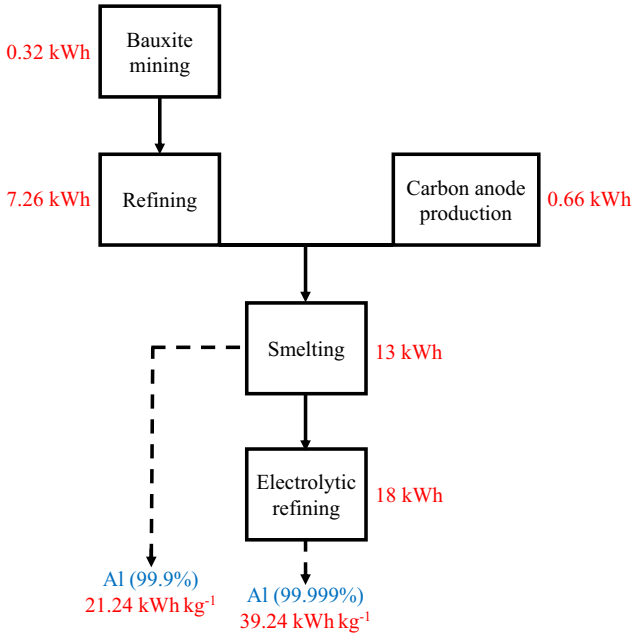

Figure 3. Average energy demand for 3N Al and 5N Al production. Reproduced under the term of the CC-5927070227651 license.[153–155] Copyright 2015, The Authors.

Another important aspect to consider is the role and influence of the protective Al (III)-oxide (Al_2O_3) layer on the Al surface.[63] The thickness of natural Al_2O_3 passivation film formed in ambient atmosphere on rolled or annealed Al foil typically ranges from 3 to 10 nm, while in fabricated artificial reinforced Al (e.g., via anodization, chemical, or plasma oxidation), the passivation film ranges from 0.1 to 5 μm.[64] Some studies suggest that the pristine Al_2O_3 layer dissolves locally in the chloroaluminate IL-based electrolyte, while others report the formation of a new oxide layer (**Figure 4**a).[27,65] This oxide layer acts as an insulator, covering the entire Al surface, impeding the interaction between the chloroaluminate IL-based electrolyte with the active Al. As a result, the formation of $AlCl_4^-$ and $Al_2Cl_7^-$ complexes is hindered.

Metallic Al undergoes plating via the chloroaluminate ion ($Al_2Cl_7^-$) and is also corroded by the same species. The corrosion causes the local dissolution of Al_2O_3 layer in the chloroaluminate IL-based electrolyte, exposing a new Al surface (Figure 4b).[66] However, some studies report that rather than releasing Al^{3+} (as $AlCl_4^-$) into the electrolyte, the pristine Al_2O_3 layer is locally dissolved, and a new oxide layer is generated (Figure 4c).[27,65] In both scenarios (whether the passivation layer dissolves or renews), several activation cycles are required to initiate the reversible redox reactions at the Al anode. Once these activation cycles are complete, the reduction and oxidation peaks, in a cyclic voltammetry, become symmetric and fully reversible. It is important to note that naked Al^{3+} ions are not present in the IL-based electrolyte. Instead, Al^{3+} is always bonded with chlorides, and its free form does not exist in this environment.[67]

Different approaches have been proposed to remove the oxide film: mechanical polishing, electrochemical polishing, or chemical etching.[38,68,69] Electrochemical polishing effectively removes the oxide layer, resulting in a smooth Al foil surface; however, this smoothness comes at a cost; after soaking the electropolished foil in chloroaluminate IL-based electrolyte for 24 h, cracks and pits form due to galvanic corrosion caused by the $Al_2Cl_7^-$ Lewis acidic complex. Interestingly, the untreated pristine Al foil, with its naturally occurring oxide film, maintains a rough and robust surface.

Some approaches to regulate the interface of Al negative electrode are the formation of an alloy (Figure 4d,e), grain refinement, surface modification, and the use of electrolyte additives.[28,70] Since electrochemical reactions take place on the surface of electrodes, the interface between the electrode and the electrolyte plays a crucial role in the electrochemical redox

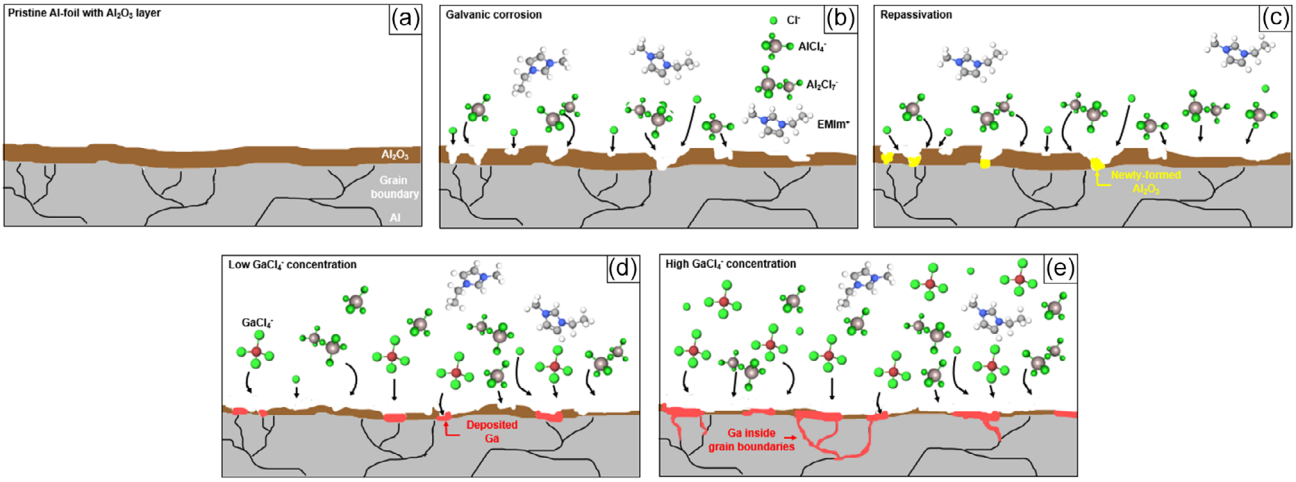

Figure 4. a–c) Schematic illustration of galvanic corrosion of the Al_2O_3 layer and passivation of the Al-foil.[156] d,e) Dependence of the $GaCl_4^-$ content for the formation of AlGa alloy and the insertion of Ga inside the grain boundaries of Al.[62]

reactions, composition, and structural changes of the Al surface which influences the ion- and mass-transport, and kinetic behavior.

Even when a relatively thick protective oxide layer exists, the Al foil is still corroded by chloroaluminate IL-based electrolyte. It has been reported that when untreated Al foils are soaked in a chloroaluminate IL-based electrolyte, after 24 and 48 h, linear cracks appear, and after 96 h, the surface becomes distorted. This degradation occurs because the native oxide film, while initially providing some protection against the acidic electrolyte, gradually breaks down, leading to corrosion. Additionally, the oxide film acts as an insulator, hindering the reduction reaction of metal salts. As a result, the electrochemical reaction area becomes increasingly limited, leading to lower capacity despite high coulombic efficiency, emphasizing the importance of oxide layer management.[68]

Choi et al.[68] demonstrated that an electropolished Al metal foil with a thin oxide layer provides a high capacity and stable surface reaction attributable to a balanced Al plating and stripping. The capacity of the untreated/pristine Al foil is limited due to the initial activation cycles. In an acidic chloroaluminate IL-based electrolyte, thinner parts of the oxide layer dissolve more quickly, restricting electrochemical reactions to localized areas; in contrast, electropolished foil enables reactions across the entire surface.[66] Rather than completely removing the Al_2O_3 oxide layer, modifying the oxide film structure is more favorable. Immersing the Al anode in the chloroaluminate IL-based electrolyte (1.3:1 molar ratio) can reconstruct the oxide layer, generating a new porous Al_2O_3 surface by partially dissolving the old film that facilitates better ion diffusion during charge/discharge processes.[66]

Dendrite formation (**Figure 5**a) is another serious issue connected to the Al_2O_3 layer. Similar to lithium, sodium, and other metal-ion batteries, dendrite formation, once started, cannot be controlled, especially at high current densities.[71] Dendrite growth leads to the formation of inactive Al (dead Al, Figure 5b), which in turn causes capacity decay and can even result in a short circuit. Gao et al.[66] discovered that an oxide layer on the Al negative

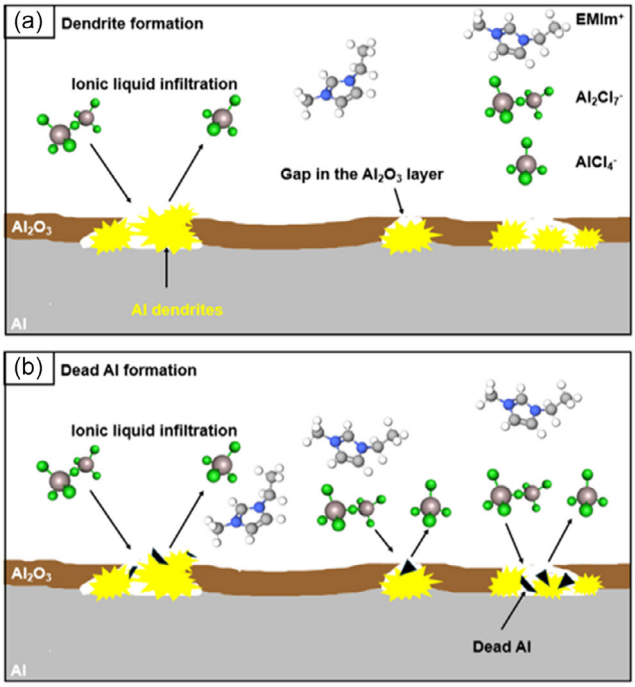

Figure 5. a) Formation of dendrites due to infiltration of IL electrolyte into gaps of the Al_2O_3 layer and b) the formation of dead Al.[157]

electrode can effectively suppress the dendritic formation. The effectiveness of this Al_2O_3 layer in preventing dendrites depends on its thickness, microstructure, and pretreatment if carried out. A thin oxide layer with a porous structure appears beneficial for RAB performance. However, despite pretreatment techniques, dendrite formation and other structural changes (such as cracks, pits, and pulverization) remain unavoidable during the charge/discharge cycles. Consequently, there is an urgent need to develop strategies to address these issues.

As seen earlier in Figure 4, alloys can stabilize the interface by inducing aluminophilic species on the electrode surface, facilitating smoother Al nucleation and growth. Inactive components

within the alloys can stabilize the lattice matrix, preventing structural collapse. The effectiveness of this stabilization depends on the individual metal compounds and their selected ratio within the alloy (Figure 4d,e). Certain alloy systems, such as Al—Ga, Al—Ti, Al—Mo, and Al—Zr, have been applied in aluminum–air batteries with promising results, which could also benefit RABs. By introducing a second or third metal, an oxide layer forms with more active defect sites; this provides additional pathways for the chloroaluminate ions from the acidic chloroaluminate IL-based electrolyte to reach the fresh Al surface with lower charge transfer resistance during plating and stripping of Al.[53,72] However, selecting the wrong alloy composition can lead to crack formation and worsen Al dendrite growth, reducing cell lifespan. This shows the importance of understanding the influence and working principles of Al alloy negative electrodes.[66]

Other aspects to consider are: 1) the volume expansion of pure and/or alloyed Al negative electrodes caused by continuous plating-alloying/stripping-dealloying reactions. This expansion can lead to pulverization of the Al electrode and loss of electrical contact. 2) the repeated breaking and formation of the protective solid–electrolyte interphase (SEI) layer consumes the electrolyte, modifying the molar ratio of $AlCl_3$:EMImCl in the chloroaluminate IL-based electrolyte, which, as stated earlier, directly affects the electrochemical activity. Meanwhile, researchers have explored Al-negative electrodes with 3D networks and/or porous structures to create physical space for mitigating/regulating the volume expansion.[66]

4. Positive Electrodes

There are several classification systems for positive electrodes for nonaqueous Al batteries. One common approach is based on the type of ion they can store and another one is based on the material type. According to the first classification scheme, the electrodes enable the insertion/deinsertion, conversion, or coordination of either chloroaluminate ions ($AlCl_4^-$)[73] or Al ions (Al^{3+}).[74] while many materials have been reported to insert Al^{3+}. However, based on our experience, a thorough analysis of these results may lead to a different interpretation. For instance, in the chloroaluminate IL-based electrolyte, Al^{3+} ions tend to form chloroaluminate ions since their high charge and small ionic radius, prevent their independent existence within the electrolyte.[22]

In the second classification system, cathodes for RABs are typically classified according to the materials employed in their fabrication, such as carbon-based electrodes, transition metal oxides, transition metal chalcogenides, polymers, MXenes, and heterostructures. In the following section, the challenges associated with each material group will be explored, rather than focusing solely on their performance; the details of the performance of some materials will be included in **Table 2**. In addition, the compounds mentioned in this section are classified in **Figure 6** according to their charge storage mechanism.

Note that even if metal-organic frameworks (MOFs) are an interesting family of compounds that are used, for instance, as a template for cathode preparation[75–77] or combined in a composite with other cathode materials,[78] they are not included in this section due to the lack of reported pure MOFs cathodes

4.1. Transition Metal Oxides (TMOs)

Transition metal oxides are among the earliest materials investigated as positive electrodes for RABs. Notably, Mn_2O_4 was reported in 2010,[79] followed by V_2O_5 in 2015 (where the authors used $AlCl_3$ and 1-butyl-3-methylimidazolium as the electrolyte).[80] However, in these early studies, stainless steel (SS) has been used in either coin cell cases or current collectors, which resulted in errors due to the electrochemical interactions between iron and chromium with the chloroaluminate IL-based electrolyte. Unfortunately, due to these experimental conditions, the reported performance values could not be considered realistic.

It is worth noting that TMOs were initially explored because, when developing new battery chemistries, researchers often draw on knowledge from established systems. TMOs, having proven highly successful in LIBs, naturally became a starting point for RAB development.

TMOs have proven to be stable when immersed in chloroaluminate IL-based electrolyte; yet, once the battery cell starts cycling, rapid capacity decay becomes noticeable. While some researchers associate this with positive material traits, such as Al^{3+} insertion or cathode–electrolyte interphase (CEI) formation, it is attributed to dissolution and loss of active material. For instance, Liu et al.[81] synthesized and tested nanosphere-rod-like Co_3O_4 and used it as positive electrode material. The specific capacity on the first cycle was 490 mA h g^{-1} at 50 mA g^{-1}; however, a fast specific capacity loss and an increase in the impedance after 20 cycles, attributed to Al^{3+} insertion, were reported. The porous microspheres of CuO reported by Zhang et al. present an initial capacity of 250 mA h g^{-1} at 50 mA g^{-1}[82] Yet, similar phenomena, both fast capacity loss and impedance increase, were interpreted as CEI and/or electrolyte decomposition. The mesoporous TiO_2 reported by Zhu et al.[83] showed an initial capacity of 125 mA h g^{-1} at 50 mA g^{-1} but a rapid capacity decay was noticed, which was also attributed to irreversible Al^{3+} insertion. Indeed, this misinterpretation often occurs. In some cases, the actual phenomenon happening is the dissolution or shuttling of the active material; this is responsible for isolating particles within the electrode and an increase in the impedance after a few cycles. Wei et al.[84] obtained an initial capacity of 90 mA h g^{-1} at 100 mA g^{-1} from MoO_2 as positive electrode. Through ex-situ examination of the separators, it was revealed that MoO_2 dissolved during cycling and transferred to the separator.

To better understand the degradation mechanisms of positive electrode materials, detailed characterizations such as elemental analysis of the Al foil counter electrode and separator after some cycles are highly encouraged. These insights may lead to better understanding and effective mitigation strategies.

4.2. Transition Metal Chalcogenides (TMCs)

Sulfides, selenides, and tellurides exhibit lower electronegativity than oxides. As a result, the reactive Al^{3+} ions undergo less

Table 2. Summary of cathode materials and their performance in RABs.

Family	Cathode	Initial specific capacity [mA h g^{-1}]	Stable specific capacity [mA h g^{-1}]	Cycle	Current density [mA g^{-1}]	Coulombic efficiency	Voltage plateaus [V]	References
TMCs	MoS_2	250	66.7	100	40	95%	0.6–0.9	[86]
	$MoSe_2$	267	117	1000	1000	>99%	1.3	[87]
	TiS_2	88	150	90	1C	>95%	0.4	[88]
	VSe_2	650	50	250	100	95%	0.6–1.2	[89]
	S	1400	600	21	251	–	0.5	[97]
	Se	180	50	50	1000	–	1.5	[98]
	Te	900	550	20	20	99	1.4	[99]
Carbon-based compounds	Graphite	60	60	7500	4000	>95%	2.0–2.2	[102]
	Graphene	85	68	8000	2000	85%	1.7	[103]
	C_{70}	750	480	100	200	≈100%	1.65	[106]
Organic compounds and polymers	Polynitropyrene-co-pyrene	260	80	1000	200	>95%	1.7	[108]
	TDPP	132	83	200	1000	>99%	1.2–1.8	[73]
	X-PVMPT	153	135	5000	2220	≈100%	0.7, 1.5	[109]
	Anthraquinone	100	85	50	50	≈99%	1.1	[163]
	Phenanthrenequinone	120	110	500	200	≈100%	1.5	[164]
TMOs	Mesoporous TiO_2	125	50	50	40	≈100%	0.7	[83]
	Coral-like TeO_2	340	91	700	200	≈80%	2	[165]
	Porous microspherical CuO	250	110	100	50	≈100%	0.8	[165]
	Nanosphere rod-like Co_3O_4	490	122	100	50	≈100%	0.8	[165]
	TiO_2	292	220	100	100	≈100%	0.4	[166]
MXenes	V_2CT_x	140	76	100	100	≈90%	1.4	[112]
	Delaminated V_2CT_x	392	90	100	100	≈96%	1.4	[112]
	$Ti_3C_2T_x$	210	75	100	100	–	1.8	[111]
	$Ti_3C_2T_x$@S@TiO_3	175	150	120	100	≈85%	1.8	[111]
	$Ti_3C_2T_x$@CTAB-Se	583	132	400	100	≈90%	2	[167]
	$CoSe_2$@NPC@$Ti_3C_2T_x$	290	220	300	1000	≈100%	2.1	[113]
Hetero-structures	MoS_2/CNF	180	53	260	100	≈80%	0.4	[168]
	WS_2/WO_3	250	200	100	1000	≈100	2	[169]
	MoS_2/rGO	390	161	100	1000	≈90%	1	[170]
	Cu_2Se/C	275	60	200	1200	≈90%	1.7	[116]

electrostatic interactions with the TMC structure, which would theoretically improve Al^{3+} ion diffusion compared to oxides. Moreover, chalcogens (S, Se, Te) have a broader range of oxidation states than oxygen (O), potentially leading to higher specific capacities through redox reactions involving more electrons. In addition, the layered structure of TMCs provides an advantage for achieving high storage capacity. However, TMCs face several challenges that impact their performance as cathodes for RABs, like their relatively low conductivity (increasing in the order $S^{2-} < Se^{2-} < Te^{2-}$) or their structural instability caused by successive (de)intercalation processes.[85]

MoS_2 is the most studied TMC cathode material, due to its layered structure and large interlayer spacing, 0.62 nm (larger than graphite's 0.32 nm); as a cathode for RABs, MoS_2 was reported to deliver a stable specific capacity of 66.7 mA h g^{-1} at 40 mA g^{-1}.[86] $MoSe_2$ is another TMC-layered material that has been widely used as a cathode. Its interlayer distance, 0.64 nm, facilitates the (de)intercalation of mobile ions. This material was also reported by Zhao et al.[87] as a cathode composite obtained by ionic complexation. It delivered an initial specific capacity of 267 mA h g^{-1} at a current density of 0.1 A g^{-1}. Another interesting TMC as cathode for RABs was reported by Hawkins et al.[88] who prepared one-dimensional (1D) TiS_2 nanobelts with sulfur vacancies. The specific capacity of TiS_2 steadily increases to 150 mA h g^{-1} after 90 cycles at 1 C rate. This was attributed to an activation process in which the intercalation of Al^{3+} between the TiS_2 layers causes the interlayer spacing to increase and the diffusion energy barrier to decrease.

VSe_2 was also regarded as an appealing cathode for RABs due to its layered structure and high theoretical capacity.[89] Lei et al. synthesized brick-like VSe_2 through a hydrothermal method. X-ray photoelectron spectroscopy (XPS) measurements

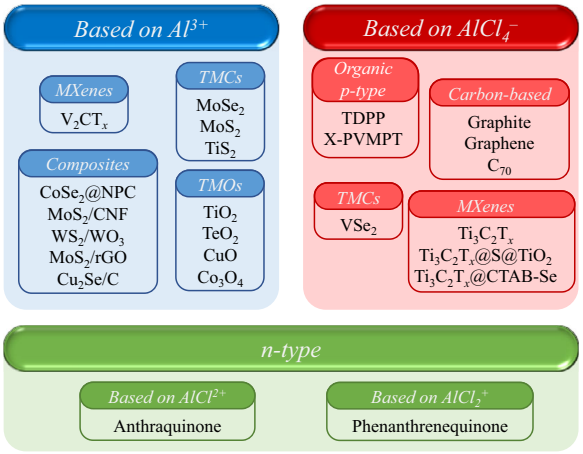

Figure 6. Classification of the cathode materials shown in Table 2 according to their charge storage mechanism.

on postmortem cathodes revealed that both V and Se experience redox reactions, thus contributing to the cell capacity. As a result, VSe_2 exhibits a high initial specific capacity of 650 mA h g^{-1} at 100 mA g^{-1} with a voltage plateau at 1.3 V. It could also retain a reversible specific capacity of 50 mA h g^{-1} after 250 cycles. However, a fast specific capacity loss is observed, decreasing from 650 to 350 mA h g^{-1} in the first four cycles and around 70 mA h g^{-1} after 50 cycles.[89] Regarding tellurides, since it is an element from Group VI, the properties of Te are similar to those of O, S, and Se. Te exhibits a strong metallic nature, causing tellurides to display relatively higher electronic conductivity. In contrast, the use of tellurium may imply sustainability issues due to its toxicity. Some of the few reported examples of transition metal tellurides as cathode for RABs are NiTe,[90] Sb_2Te_3,[91] and $Cu_{1.81}Te$.[92]

A concerning challenge with TMCs cathode material is the dissolution of the active material within the chloroaluminate IL-based electrolyte during cell operation, due to its strong Lewis acidic nature which can be observed as a rapid specific capacity decay. In the case of sulfides, electrochemical activity causes sulfur atoms to be arranged in chains, the so-called polysulfides. The high-order polysulfides, that is, long chains of S_n^{2-} ($n \geq 6$) are soluble in the chloroaluminate IL-based electrolyte.[93] During the electrochemical oxidation of Se^{2-} to Se^{4+} from selenides, selenium tends to coordinate with the $AlCl_4^-$ ion present in the electrolyte to form the soluble species Se_2Cl_2.[94] Similarly, tellurides undergo dissolution in the electrolyte even without cell operation: $AlCl_4^-$ ions are prone to interact with Te^{2-} ions to form the soluble complex AlTeCl.[95] As a result, these soluble species can undergo a shuttle effect and diffuse through the separator, causing a progressive loss of the active material from the electrode and thus, an irreversible capacity fading, hindering the electrochemical performance of TMCs.

To alleviate the dissolution of TMCs, two main strategies have been followed as illustrated in **Figure 7**: heterostructures and modified separators. Heterostructures focus on enhancing structural stability, providing a robust framework to minimize material loss (further studied below). In contrast, modified separators, often incorporating carbon-based materials such as nanotubes[90] or CMK-3 (carbon mesostructured by KAIST)[96] are designed to

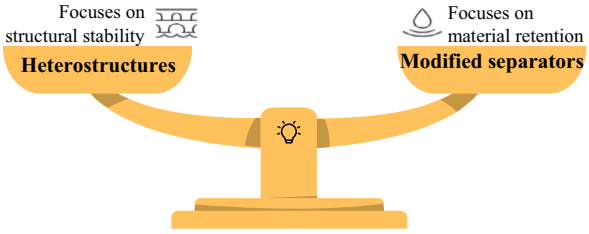

Figure 7. Strategies to alleviate the dissolution of TMCs.

retain TMCs within the cathode. This retention prevents material loss due to the shuttle effect, ensuring that soluble compounds generated during the electrochemical oxidation reaction can be efficiently reduced back. Based on the studies presented, it is recommended to evaluate the dissolution and chemical reactivity of candidate cathode materials in the electrolyte before the preparation of the cells.

It is important to mention that pure chalcogens can be also employed as cathodes for RABs, see Al–S,[97] Al–Se[98] and Al–Te[99] batteries. However, they suffer from dissolution phenomena, leading to fast capacity decay or short cycle life, unless strategies for avoiding this issue such as the ones explained above are taken. As in all rechargeable battery systems, their electrochemistry involves both reduction and oxidation reactions.[100]

4.3. Carbon-Based Compounds

Carbon-based compounds are the most employed cathode for RABs with chloroaluminate IL-based electrolyte. They exhibit good structural stability and cycling performance, while their production costs are low due to their availability. However, in some cases, such as graphite, production is largely concentrated in a few regions of the world, raising sustainability concerns. Moreover, relying on the intercalation of anions, they operate at high electrochemical potential. Additionally, since their charge storage mechanisms rely solely on intercalation of $AlCl_4^-$, these materials deliver low capacity values.[101]

Graphite can be considered the most used cathode for RABs: in 2015, it was the first carbon-based material that exhibited electrochemical activity, with excellent cycling stability and rate performance as a cathode for RABs.[102] It was prepared as a three-dimensional (3D) graphite foam through vapor deposition and it delivered a specific capacity of around 60 mA h g^{-1} at 4 A g^{-1}, displaying a high voltage plateau in the region of 2.25 V. Such voltage makes graphite one of the highest voltage operating cathodes for RABs. However, the voltage stability window of the electrolyte (up to ≈2.5 V) limits the electrochemical performance of graphite, precisely due to its high operating voltage. After 7500 cycles at the same current density, capacity decay was barely observed.

Graphene has an ideal structure for the transport of electrons or ions: it consists of single layers of carbon atoms arranged in a two-dimensional (2D), hexagonal structure and linked through $\pi-\pi$ bonds, enhancing the carrier mobility. It is between the 2D layers where the $AlCl_4^-$ ions are intercalated. In the past years, modifications have been made to graphene: for instance,

Qiao et al.[103] prepared a defect-free, self-supported graphene cathode that delivered a specific capacity of 85 mA h g^{-1} at a current density of 2 A g^{-1}, with only 20% capacity loss after 8000 cycles.

Carbon-based compounds can exhibit less common charge storage mechanisms as well. For instance, carbon nanotubes can store energy via an electric double-layer adsorption mechanism.[104] Fullerene like C_{60} has also been reported to show an adsorption mechanism; due to its large size, $AlCl_4^-$ ions cannot penetrate the cavities on the surface of fullerene; instead, the charge storage mechanism relies on reversible (de)adsorption of $AlCl_4^-$ on the surface. However, the specific surface area of fullerene is moderate, which limits the delivered specific capacity to 78 mA h g^{-1}.[105] Another proposed charge storage mechanism for carbon-based compounds is a direct complexation. Huang et al.[106] reported that C_{70} fullerene follows this mechanism, leading to the formation of the complex $C_{70}{\cdot}[AlCl_4]_xCl_{n\text{-}m}$.

4.4. Organic Compounds and Polymers

Recently, some organic compounds and conducting polymers have received attention as cathodes for RABs.[73] Usually, these compounds exhibit p-type redox activity, i.e., they can be oxidized by coordination of $AlCl_4^-$. The main challenge related to organic compounds and polymers is their limited conductivity. Some of the first compounds of this family proposed as cathode for RABs were polypyrrole and polythiophene.[107] After some years, Kovalenko et al. demonstrated the benefits of employing long-chain polymers rather than light, single organic molecules, since long chains possibly alleviate the problem of low conductivity by promoting the delocalization of π-electrons across the polymer chain.[108] As a result, porphyrin-derived thienyldiketopyrrolopyrrole (TDPP) delivered a reversible capacity of 83 mA h g^{-1} after 200 cycles at 1 A g^{-1} with an excellent capacity retention (97%).[73] Cross-linked poly(3-vinyl-N-methylphenothiazine) (X-PVMPT) is another example of polymer as cathodes for RABs with promising electrochemical performance. X-PVMPT delivered a specific capacity of 83 mA h g^{-1} after 200 cycles at 1 A g^{-1}, displaying good cycling stability (**Figure 8**).[109]

4.5. MXenes

MXenes have emerged as promising candidates not only for RABs but also for other applications. Their tunable compositions and properties have earned significant attention, offering a wide and versatile range of possibilities for electrode design.[110]

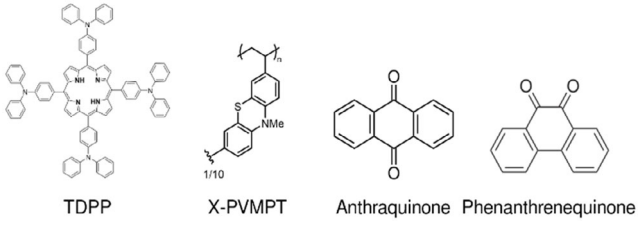

Figure 8. Structure of the organic/polymeric cathodes mentioned in this review.

Particularly in the context of nonaqueous Al batteries, the surface groups of MXenes play a decisive role in influencing their performance as cathodes for RABs. Understanding these surface interactions is crucial for using the full potential of MXenes as cathode materials. The positive charge of Al^{3+} would strongly interact with the negatively charged functional groups on the MXenes surface through electrostatic attraction; the electronegativity of the surface groups like fluorine (—F) and oxygen (—O), would influence the strength of this interaction.

Consistent with this, Huo et al. studied the possibility of using delaminated $Ti_3C_2T_x$ (MXene) as a positive electrode for RABs,[111] obtaining an initial specific charge capacity of 210 mA h g^{-1} at 100 mA g^{-1} but with an initial efficiency of only 31%. The authors attribute the low coulombic efficiency to irreversible interactions of the termination groups with the intercalating ions and the blocking of active positions in the cathode. In their study, Mohammadi et al. compared multilayered MXene with few-layer V_2CT_X MXenes intercalated with tetrabutylammonium hydroxide (TBAOH).[112] The findings reveal that the delaminated material exhibits performance up to twice as high as the multilayered counterpart (392 vs 140 mA h g^{-1} at 100 mA g^{-1} at the first cycle). This enhancement is attributed to the uniformity achieved in the delamination process of the layered material when TBAOH is utilized. The delaminated material shows impressive stability during cycling as it has one of the lowest capacity losses among reported materials. The author suggests that the small change in the lattice parameter of the delaminated material is due to the intercalation of the small Al^{3+} ion and compares this behavior to the one presented when the intercalated ion is Na^+. In this context, it is important to note that when Al^{3+} is suggested as the intercalating ion, not only its ionic radius but also its electrostatic interactions with the host structure should be considered; therefore, this kind of comparison is considered risky.

MXenes have not only been utilized as the active material but have also found primary application in positive electrodes for RABs within synergistic heterostructures, studied in more depth in the following section. In these configurations, the two-dimensional, highly conductive materials offer stability, buffer volume changes during cycling, and prevent the dissolution and shuttling of the active material. For instance, $Ti_3C_2T_x$ has been employed by Yao et al. to mitigate excessive loss of active species and structural pulverization of cobalt sulfide and cobalt selenide,[113] maintaining specific capacities of 111 mA h g^{-1} after 1000 cycles and 220 mA h g^{-1} after 300 cycles, respectively, at 1 A g^{-1}.

4.6. Heterostructures

Heterostructures in positive electrodes for RABs are generally used to overcome challenges such as rapid capacity loss due to decomposition/dissolution of the active material. For instance, as stated earlier metal chalcogenides usually suffer from structural instability, volume expansion, poor electrical conductivity, and capacity decay. Heterostructures are commonly reported alongside their constituents, which are often modified to achieve the desired heterostructure configuration. At heterogeneous interfaces, the Van der Waals forces between different atoms

can induce lattice distortion. Additionally, variations in band energies between different materials in heterostructures lead to electron transfer, creating a built-in electric field that accelerates reaction kinetics and enhances structural stability.[101]

In this order of ideas, the study by Zhuang et al.[114] provides further evidence supporting the hypothesis that the high conductivity and mechanical stability of carbon nanofibers create a stable network for cobalt sulfide. This network reduces the specific capacity loss during cycling associated with volume changes and eliminates the need for binders, along with the associated issues. The material maintains a specific capacity of near 80 mA h g^{-1} after 500 cycles at a current density of 200 mA g^{-1}. In the same way, MXenes have been used to hinder the pulverization of active material and increase cyclability; reduced graphene oxide has been proposed by Cai et al.[115] as a wrapping layer for cobalt selenide/carbon nano-dices; the final material ($CoSe_2$/C-ND/rGO) has proven to suppress the dissolution of cobalt species and enhance the cycling stability, maintaining a specific capacity of 143 mA h g^{-1} at 1000 mA g^{-1} after 500 cycles.

One of the strategies used to buffer volume expansions and improve electrical conductivity is the encapsulation of active material in 3D porous carbon, like what was proposed by Li et al.[116] with copper selenide. Even Cu_2Se@C maintains a specific capacity of 54.4 mA h g^{-1} at 800 mA g^{-1} after 200 cycles, the sharp capacity loss after the first ten cycles, characteristic of chalcogenide-based electrodes is still observed. A behavior similar to this is the one reported by Wang et al.[116] who proposed a self-standing electrode made of molybdenum disulfide (MoS_2) and carbon nanofibers in a sandwich-like arrangement to support the active material, reduce its agglomeration, and alleviate the volume expansion; the initial specific capacity reported was 180 mA h g^{-1} which quickly decreases to around 55 mA h g^{-1} after 10 cycles at 100 mA g^{-1}.

It can be observed that while heterostructures often exhibit higher specific capacities than their constituents, they may either address the deficiencies of the original structure or retain the challenges associated with its components, such as dissolution and shuttling of active material. Nevertheless, they still demonstrate improved performance. Encouraging further research in this direction is crucial, as heterostructures show promising properties as a viable approach to achieving stable, reversible positive electrodes for RABs.

5. Binders

In RABs, selecting an appropriate binder material is critical for maintaining electrode integrity and optimizing electrochemical performance. Undesired degradation can occur if the binder decomposes/dissolves in the electrolyte. Therefore, an inert active material should be used in combination with an unreactive binder.

Polyvinylidenfluorid (PVdF) is widely employed as a binder (commonly used in LIBs manufacturing) due to its piezoelectric properties, thermal stability, mechanical strength, and chemical resistance against acids, bases, aromatic solvents, and oxidizing agents.[117] However, it has two significant weaknesses: 1) strong bases and 2) organic amines, both of which gradually cause dehydrofluorination (DHF), resulting in the formation of hydrofluoric acid (HF) and sp^2 carbon–carbon double bonds in the polymer chain.[118,119] As it can be observed in **Figure 9**, when exposed to the acidic chloroaluminate IL-based electrolyte, the white PVdF powder turns black, indicating side reactions with $Al_2Cl_7^-$.[79,119–121]

Chen et al.[122] observed the decomposition of the $-CF_2$ group in PVdF using XPS. Surprisingly, their electrochemical systems based on cobalt boride (CoB) and reduced graphene oxide dried under supercritical conditions (RGOCPD) showed no adverse effects.[117,121] Smajic et al.[121] observed similar outcomes for RGOCPD used as a positive electrode for RABs in an IL electrolyte. However, a detaching or delamination effect of the active material from the current collector was reported.[117] Additionally, in 2015, Wang et al.[80] highlighted the dissolution of PVdF in the IL-based electrolyte, resulting in a significant decrease in electrochemical performance.

In 2022, Yu et al.[123] introduced pencil-drawing graphite nanosheets (PGN) as the positive electrode, coating PVdF on the surface to enhance cathode stability during the volume expansion caused by $AlCl_4^-$ intercalation. Rate capability tests of PGN with and without a PVdF layer showed a significant difference. Without PVdF, the initial cycle at 0.5 A g^{-1} exhibited a specific discharge capacity of ≈45 mA h g^{-1}, whereas PGN with PVdF delivered ≈72 mA h g^{-1}. This trend of higher charge/discharge capacities continued at 1.0, 2.0, and 5.0 A g^{-1}. Additionally, with a PVdF layer on the electrode, charge and discharge capacities slightly increased with more cycles at all current densities. After returning to a current density of 0.5 A g^{-1}, the PVdF-based electrode delivered ≈94 mA h g^{-1}, while the PGN electrode without PVdF returned to its initial value. However, the same authors noted PVdF dissolution during the initial cycles. Z. Yu et al.[124] reported the deactivation of the IL electrolyte by adding 2.5 wt% of PVdF. After the thermal side reaction, Raman spectra confirmed the disappearance of $AlCl_4^-$ and $Al_2Cl_7^-$ bands. Yang et al.[125] demonstrated higher cycle stability for

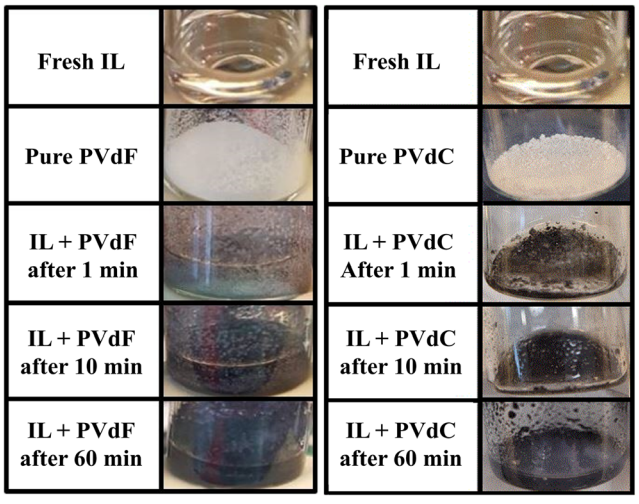

Figure 9. Time relating optical change of PVdF and PVdC binder material in contact with $AlCl_3$:EMImCl (1.5:1) chloroaluminate IL-based electrolyte.[126]

sodium-alginate (Na-Alg) graphite electrodes at 1000 mA g^{-1} compared to PVdF-based ones. The dissolution and disappearance of $-CF_2$ groups of PVdF are reasons mentioned to be responsible for decreasing capacity. In summary, the use of PVdF as a binder material in RABs has led to three distinct interpretations regarding its impact on side reactions. First, some studies suggest that the reaction between PVdF and the $AlCl_3$:EMImCl electrolyte does not significantly impair performance. Contrarily, others find that unwanted side reactions and the dissolution of the binder can negatively affect electrochemical performance. Interestingly, yet another interpretation suggests increased specific capacity and enhanced electrode stability despite binder dissolution.

Zemlyanushin et al.[126] further investigated PVdF and polyvinylidene chloride (PVdC) and explained the side reactions of DHF (**Figure 10**a) and dehydrochlorination (DHC), respectively. The measured Raman spectra of soaked binders confirmed that the PVdF and PVdC act like amorphous carbon precursors (Figure 10b). For both reacted polymers, typical D- and G-bands were visible in the Raman spectra. PVdC, in particular, demonstrated similar Raman spectra after induced DHC by laser irradiation, highlighting the reactivity of the chloroaluminate IL-based electrolyte. DHF and DHC in PVdF and PVdC lead to the formation of aluminum tetrafluoride (AlF_4^-), hydrofluoric acid (HF), and hydrochloric acid (HCl), respectively, as illustrated in Equation (3)–(5).

$$\text{PVdF: } 2(C_2H_2F_2)_n + nAl_2Cl_7^- \rightarrow 4nC + nAlF_3 + nAlCl_4^- + nHF + 3nHCl \quad (3)$$

$$AlF_3 + HF \rightleftharpoons AlF_4^- + H^+ \quad (4)$$

$$\text{PVdC: } (C_2H_2Cl_2)_n + 2Al_2Cl_7^- \rightarrow 2nC + 2nAlCl_4^- + 2nAlCl_3 + 2nHCl \quad (5)$$

The $-CF_2$ group in PVdF-based electrodes decomposes upon contact with chloroaluminate IL-based electrolyte as evidenced by XPS.[117] This finding aligns with ^{19}F-NMR results, indicating that the newly formed species dissolve in the electrolyte.[126] Electrochemical tests (**Figure 11**) indicate PVdF to be the better binder material for graphite-based RABs. Compared to PVdC, PVdF shows a lower polarization, higher specific capacity, and increased stability. Specifically, the formed AlF_4^- can intercalate into graphite.[126] However, a further side reaction occurs when the intercalation product (C_xAlCl_4) reacts with formed hydrofluoric acid (HF), as shown in Equation (6).[127] Therefore, the formed HF can damage the graphite structure and even worsen the corrosion problem. In contrast, Wang et al.[128] predicted that the use of AlF_4^- as an active species in RABs will lead to larger cathode-specific capacity, higher voltage, and higher rate capability.

$$C_xAlCl_{4(s)} + 4HF_{(l)} \rightarrow (x - 0.25)C_{(s)} + AlF_{3(s)} + 4HCl_{(g)} + 0.25CF_{4(g)} \quad (6)$$

Water-based carboxymethyl cellulose (CMC) avoids critical solvents like N-methyl-2-pyrrolidone (NMP). However, it reacts similarly to PVdF in the chloroaluminate IL-based electrolyte. Moreover, intermolecular interactions between $AlCl_4^-$ and $Al_2Cl_7^-$ ions and CMC hydroxyl (—OH) groups hinder charge transfer.[129] CMC also undergoes cross-link reactions, resulting in gelling probably initiated by the great ability of $AlCl_4^-$ as a catalyst for such reactions.[130] Uemura et al.[120] investigated various binder materials via Fourier-transform infrared (FTIR) spectroscopy. The only materials that did not react with the electrolyte were polyimide (PA), polysulfone (PS), and polytetrafluoroethylene (PTFE). PTFE is chemically stable but hard to handle. The mass and thickness of positive electrodes are difficult to maintain consistently for direct comparison of electrochemical results. Problems like the correct optimization of used cathode–anode mass balance, to build a functional full cell, will occur after finding suitable housing, binder, cathode, and anode materials or their modifications. For example, Huang et al.[131] reported that in RABs, a high graphite loading leads to lower capacity because the higher volume hinders the smooth diffusion of $AlCl_4^-$ into the host material. For comparison, Appiah et al.[132] discovered that in the chloroaluminate IL-based electrolyte the optimal thickness for a graphite electrode (90% graphite + 10% PVdF binder) is 50 μm. A thicker positive

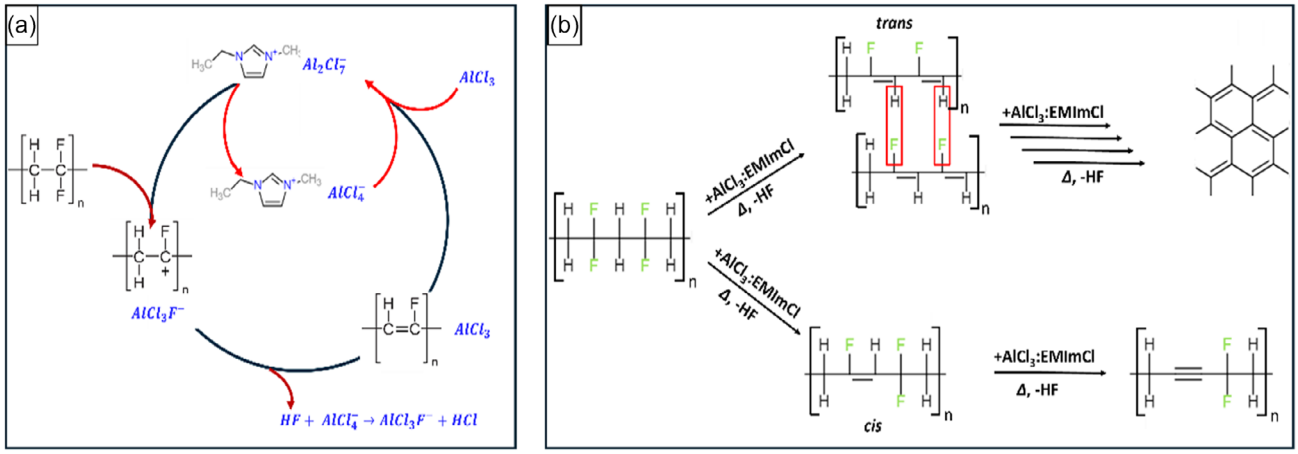

Figure 10. Schematic illustration of a) the DHF of PVdF and b) the formation of carbon-rich species as well as polyyne due to the DHF of PVdF.[126]

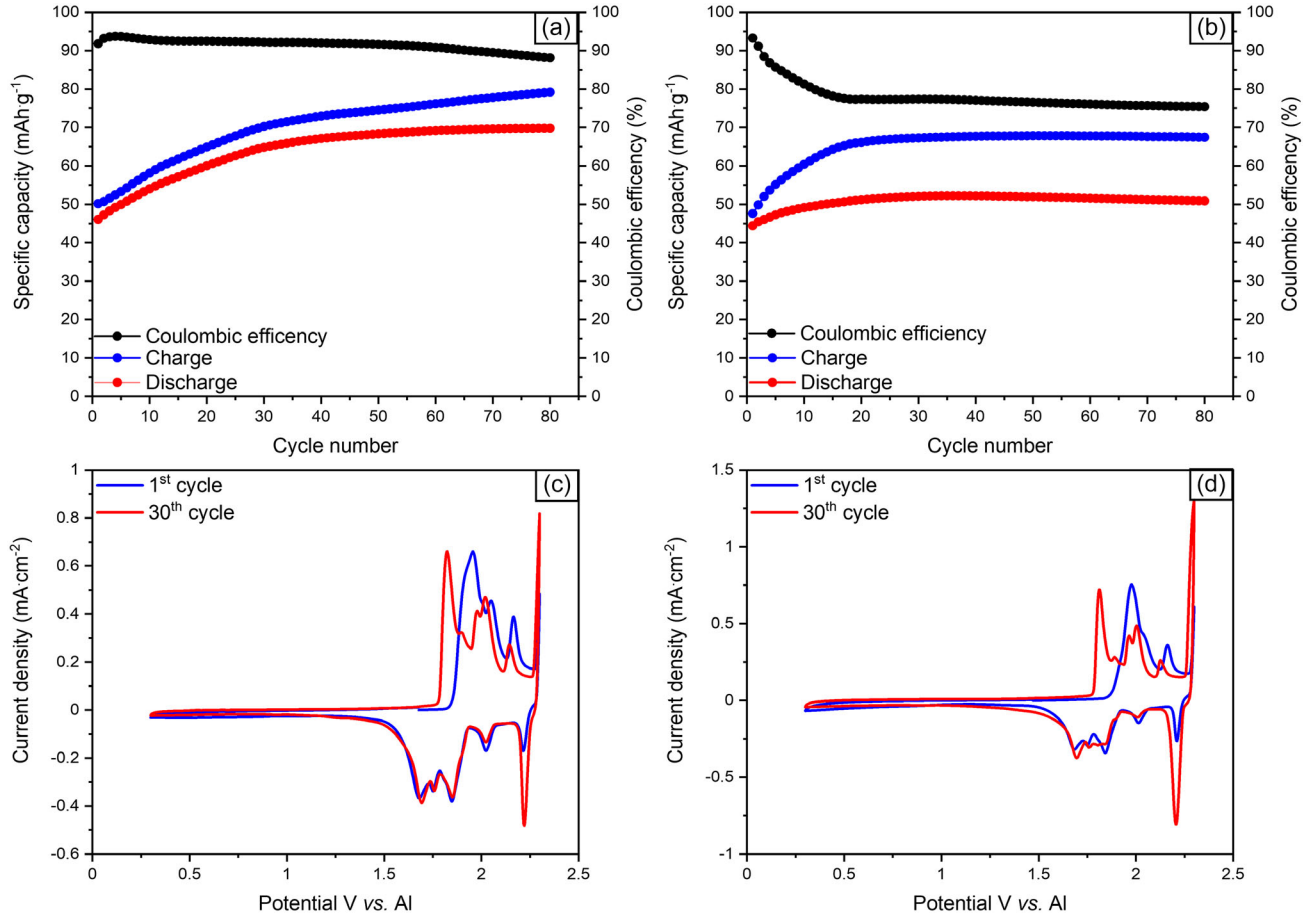

Figure 11. GCPL of a) PVdF and b) PVdC and cyclic voltammograms of c) PVdF and d) PVdC. Reproduced under the term of the CC-4.2 license.[126] Copyright 2024, The Authors.

electrode would increase the diffusion time of $AlCl_4^-$ and prevent complete (de)intercalation. By using thick electrodes, the chloroaluminate IL-based electrolyte molar ratio decreases, and the remaining active species inside the graphite layers block intercalation pathways. Consequently, the charge/discharge capacities become lower.

6. Laboratory-Scale Technical Challenges in RABs Research

In battery technology research, the study of each cell component begins with the development of new electrodes, electrolytes, additives, interfaces, and coatings, requiring a deep understanding and thorough investigation. This process starts with the synthesis and evaluation of the structure and composition, followed by ex-situ and post-mortem characterizations such as X-ray diffraction (XRD), XPS, Raman spectroscopy, SEM, thermogravimetric analysis (TGA), and FTIR. These characterizations typically include electrochemical tests to assess performance. Based on these results, advanced analytical techniques are employed to understand the mechanisms occurring during electrochemical cycling. Understanding the dynamic behavior of electrodes and electrolytes through operando measurements is also crucial. Techniques such as XRD or synchrotron radiation diffraction (SXRD) are essential for studying the intercalation of Al complexes, X-ray absorption spectroscopy (XAS) is crucial to understanding the variation of the oxidation state of metal centers during charge and discharge; while in situ Raman spectroscopy provides insights into electrolyte composition and stability during charge/discharge cycles, additionally, near ambient pressure XPS can offer valuable information on SEI formation or electrolyte decomposition on the surface of the negative electrode. However, applying these characterization techniques and conducting electrochemical measurements is particularly challenging in RABs research with the existing setups.

The corrosive nature of chloroaluminate IL-based electrolytes is necessary to erode the Al_2O_3 passivation layer on the metallic Al anode exposing it to subsequent Al plating/stripping,[133,134] however, corrosiveness is one of the challenges that arise during characterization and electrochemical measurement in RABs.[135]

The corrosivity of the chloroaluminate IL-based electrolyte can impact research on RABs in two significant ways. First, it can influence the performance of the negative and positive electrodes, as well as other passive components within the cell. Second, it can hinder the research process itself, causing issues during experiments and material characterization. Here, we briefly discuss both categories, drawing from existing literature

in the RABs research field and experiences from our team. The challenges associated with the technical aspects of researching RABs are also illustrated in **Figure 12**.

6.1. Challenges in Electrochemical Evaluation of RAB Systems

Performing any electrochemical measurement to evaluate the electrochemical behavior of RAB systems faces significant challenges due to the corrosive nature of the chloroaluminate IL-based electrolyte. As stated earlier, when performing the electrochemical measurement, all parts of the cell should be stable under the conditions in which the test is conducted. Finding a cell type that is compatible with the corrosivity of the chloroaluminate IL-based electrolyte is crucial for improving measurement reliability and durability while avoiding issues such as corrosion and measurement inaccuracies. As depicted in **Figure 13**, alternative materials and designs offer significant advantages over conventional approaches.

Conventional SS coin cells are unsuitable due to corrosion in the presence of this electrolyte. To prevent corrosion, metal rods from Swagelok cells and SS components must be replaced with unreactive material; the perfluoroalkoxy (PFA) body of the Swagelok cells is stable in acidic and alkaline environments. Additionally, the SS coin cell crimping machine, essential for sealing these cells, is also susceptible to destruction upon contact with the acidic electrolyte.

Glass cells offer a more inert option as glass does not react with Lewis acidic chloroaluminate IL-based electrolytes. Alternatively, cell parts can be manufactured from Inconel alloy or PTFE. Unstable components may be coated with titanium nitride (TiN) or chromium nitride (Cr_2N).[136]

Another approach (adopted by our group) to investigate the electrochemical performance of RABs is the adoption of different test cells proposed by rhd instruments,[137–139] which are named TSC1600 (**Figure 14**a), TSC Surface (Figure 14b) advantageous when using large electrolyte volumes) and TSC Battery

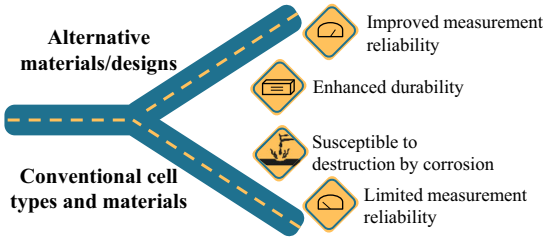

Figure 13. Evaluation of material and design for electrochemical characterization of RABs.

(Figure 14c) for testing acidic electrolytes with various types of Al foils and/or cathode materials, respectively. The cells are made from polyether ether ketone (PEEK) and use glassy carbon (GC) as the current collector. The PEEK is very stable in contact with acidic and alkaline environments, although its moisture absorption requires careful drying.

6.2. Challenges Regarding the Stability of Current Collectors with the Electrolyte

Standard current collectors made of pure metals, which should have chemical, electrochemical, thermal, and mechanical stability, and good electronic conductivity, are often reactive with the chloroaluminate IL-based electrolyte and therefore unsuitable for RAB characterization.[117] The anodic stability of metal CCs within the voltage range of 0–2.5 V versus Al in an acidic chloroaluminate IL-based electrolyte was evaluated for Cr, SS, Al, titanium (Ti), gold (Au), GC, and molybdenum (Mo). None of these materials were found to be stable, and they are not recommended due to their reactivity.[136]

Avoiding side reactions is crucial as they can introduce incorrect additional capacities, complicating the fair comparison of material performance.[69] For instance, it has been demonstrated that SS, composed of iron (Fe) and Cr, used in coin cells and current collectors, undergoes redox reactions with the electrolyte, resulting

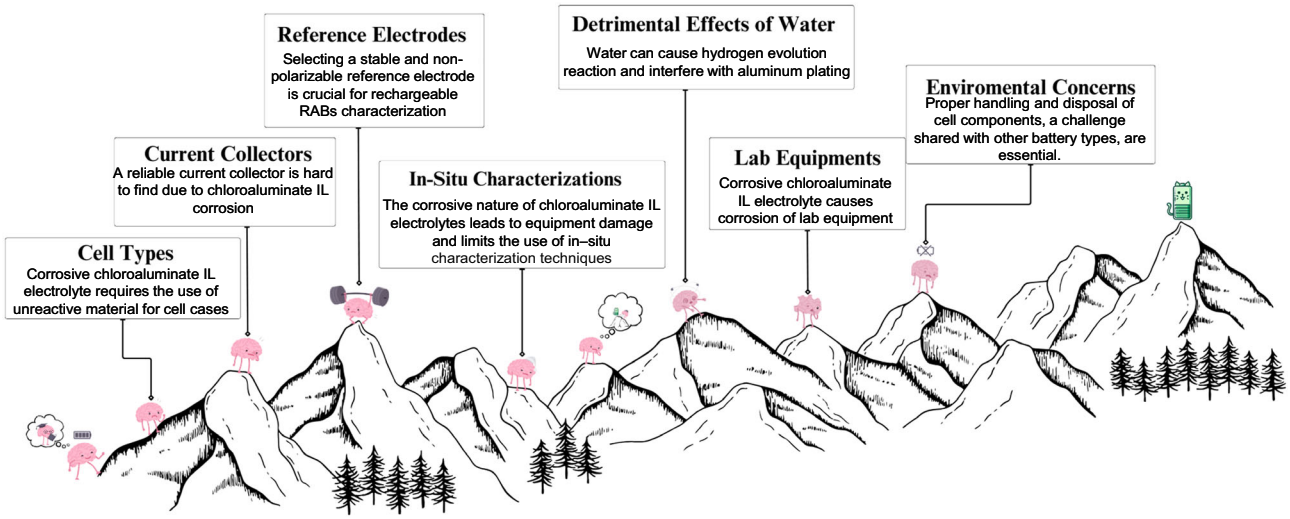

Figure 12. A graphical illustration depicting the challenges encountered in the research and development of rechargeable aluminum batteries. This figure was generated using Canva.

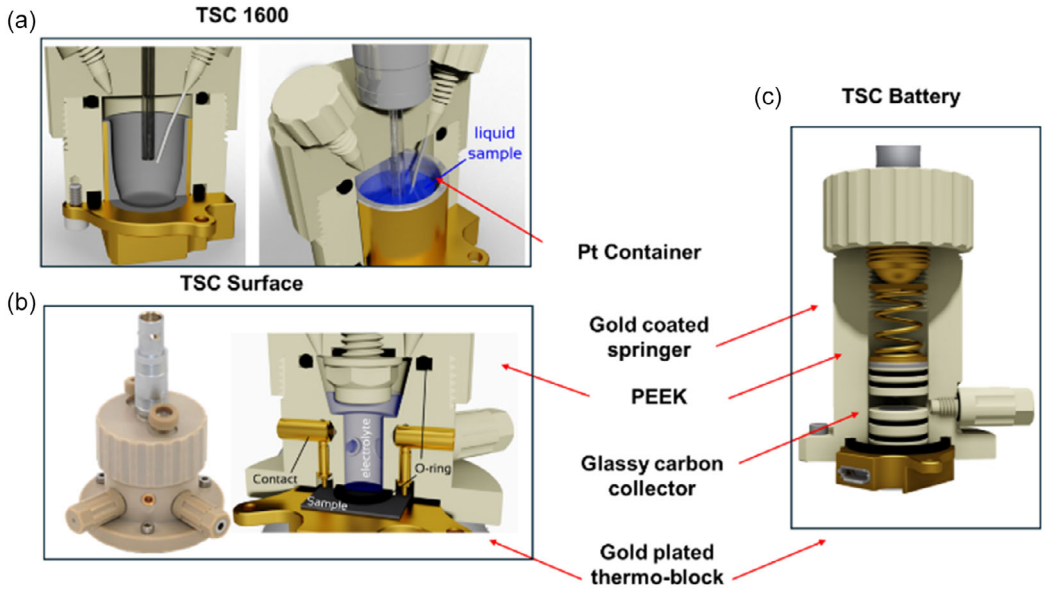

Figure 14. a) Core of TSC 1600 cell for electrolyte testing, b) TSC surface, and c) TSC battery.[137–139]

in capacity generation (Equation (7), (8)). Moreover, the positive electrode active material, vanadium (V) oxide (V_2O_5), also participates in these unwanted reactions.[12] Further investigations have demonstrated the reactivity of nickel (Ni) (Equation (9)).[37]

$$4AlCl_4^- + Fe \rightleftharpoons 2Al_2Cl_7^- + FeCl_2 + 2e^- \quad (7)$$

$$4AlCl_4^- + Cr \rightleftharpoons 2Al_2Cl_7^- + CrCl_2 + 2e^- \quad (8)$$

$$xNi^{2+} + 4(1-x)Al_2Cl_7^- + (3-x)e^- \rightleftharpoons Ni_xAl_{1-x} + 7(1-x)AlCl_4^- \quad (9)$$

The corrosion of Mo rods in contact with the chloroaluminate IL-based electrolyte is illustrated in **Figure 15**a,b. Furthermore, Figure 15c,d shows that the chloroaluminate IL-based electrolyte in a molar ratio of 1.5:1 changes color from light yellow to red after being cycled in contact with a Mo metal source. Zemlyanushin et al.[140] demonstrated the dissolution of Mo which results in the formation of several different oxidation states with paramagnetic unpaired electron constellation. In addition, cyclic voltammetry (CV) and galvanostatic cycling with potential limitation (GCPL) measurements result in redox activity leading to additional generated specific capacity.[140] Moreover, a possible reaction mechanism of Mo (**Figure 16**) has been postulated, based on the comparison of our own results and the results of Jiao et al.[99] and Zhang et al.[95] on Al—Te (tellurium) batteries.

Unfortunately, using Mo as a current collector in RABs research can introduce potential errors in performance evaluation. Therefore, considering that many groups still work with Mo as a current collector,[3] caution is advised when interpreting research results involving Mo current collectors. Tungsten (W), titanium nitride (TiN), and chromium nitride (Cr_2N) are suggested to be stable in chloroaluminate IL-based electrolyte.[136]

Further research has shown that tantalum (Ta) and poly(ethylene terephthalate) (PET) coated with indium tin oxide (ITO) are

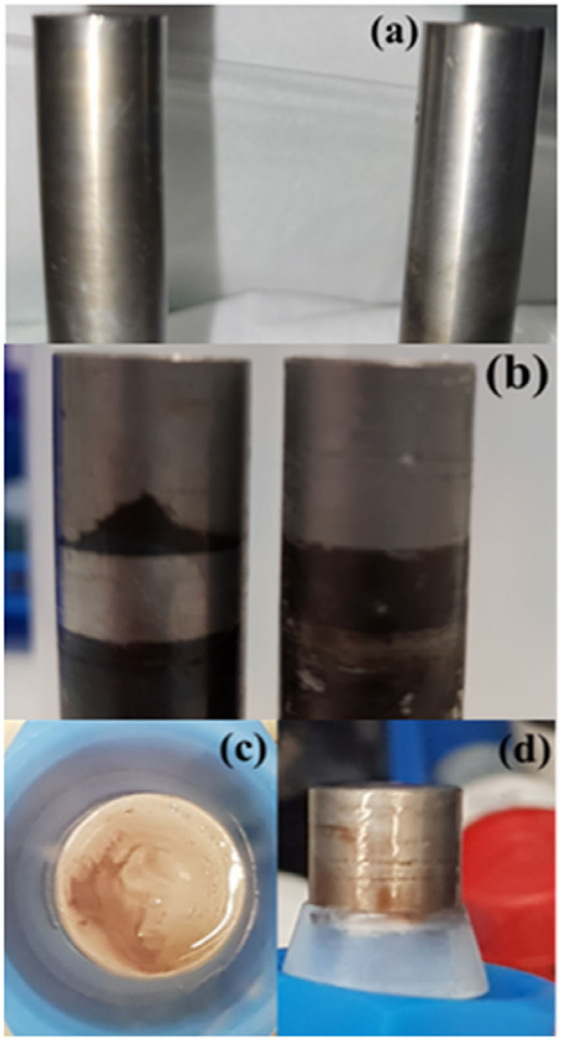

Figure 15. a) Mo rods before cycling, b) Mo rods, c) top, and d) side view of the Mo rod after cycling.

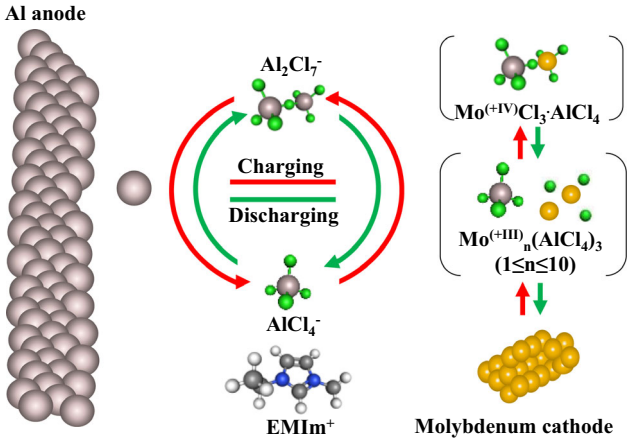

Figure 16. The proposed working mechanism of Mo-foil in $AlCl_3$-based RAB.

stable up to 2.75 V versus Al. Consequently, polyimide sputtered with TiN or Cr_2N and PET coated with ITO are currently the best current collector systems for RABs. These materials are easy, inexpensive to fabricate, and are significantly more stable at high voltages compared to commonly used metallic CCs.[117]

In some cases, GC rods or discs have been used as current collectors in Swagelok cells. Glassy carbon's shiny surface makes it easy to clean and polish and its tight atomic bonds prevent penetration or insertion of external compounds,[141] giving it self-protective properties against corrosion, weathering, alkali, and acid.[142] Despite these advantages, glassy carbon is brittle and susceptible to fracture under tensile stress.[143] Additionally, debris can be removed from the rod and trapped inside the cell when pressure is applied to close the Swagelok cell, posing another challenge for testing RAB components. In this case, glassy carbon may be a viable option for research but not for scaling up or commercial prospects.

6.3. Challenges in the Selection of Reference Electrodes

Accurate electrochemical measurements rely on choosing a reference electrode that remains stable, maintains consistent composition throughout measurements, and remains nonpolarizable to ensure a stable potential. However, this selection process depends heavily on the specific electrolyte composition and experimental conditions.

Conventional reference electrodes, such as the saturated calomel electrode (Hg/Hg_2Cl_2) or Ag/AgCl electrode, are designed for aqueous environments and are unsuitable for nonaqueous systems. These electrodes may exhibit unpredictable behavior or potential drift, rendering them incompatible with commonly used electrolytes in rechargeable batteries. As a result, researchers often turn to pseudo-reference electrodes, even though they may yield irreproducible potentials under specific conditions. For example, Na metal electrodes in Na-ion batteries provide unstable and poorly reproducible voltage measurements. To address this issue, research in these fields has explored alternative reference materials, including silver wire, activated carbon, and metal alloys.[144–146]

In RABs with chloroaluminate IL-based electrolyte, conventional pseudo-reference electrodes like silver (Ag) or Pt wire are discouraged due to instability and potential drift in the corrosive electrolytes, as depicted in **Figure 17**. Even Al wire presents challenges due to a surface passivation layer that can be affected by different electrolytes, especially in the presence of water residue, hindering accurate measurements. These limitations underscore the need for further exploration of reference electrodes specifically tailored for RABs research. Researchers must seek solutions that address the unique demands of these systems to enhance the accuracy and reliability of electrochemical measurements.

6.4. Challenges with Operando and Postmortem Characterizations of RABs

A significant limitation in RAB research is the difficulty of directly observing real-time interactions. Corrosion poses a considerable risk, leading to cell leakage and potential damage to expensive equipment. Unfortunately, this limitation hinders the widespread adoption of operando techniques. For instance, during an attempt to prepare an in situ cell in our lab, the crimping machine corroded, and the Kapton window was destroyed, resulting in electrolyte leakage. Similar issues were encountered during in situ Raman experiments. Although corrosion-resistant PEEK cells are available on the market, operando or in situ experiments often require a penetrating window, complicating the design and setup. While pouch cells allowed beam penetration and transmission for operando synchrotron XRD and XAS measurements, we also encountered electrolyte leakage during the transportation of some cells.

Beyond the corrosion challenges associated with operando techniques, it is crucial to emphasize the need for a comprehensive approach when characterizing Al^{3+} or chloroaluminate ion intercalation in cathode materials. Relying solely on one or two characterization methods may lead to erroneous conclusions due to the complex nature of intercalation processes and the limitations of individual techniques. Researchers must adopt a multifaceted strategy to confidently confirm Al^{3+} intercalation/insertion and understand its implications for battery performance and stability.

Furthermore, specific techniques, such as XPS and energy-dispersive X-ray spectroscopy (EDS), face challenges in distinguishing between inserted Al species and chloroaluminate ions originating from the electrolyte. Particularly when assessing surface compositions, both inserted Al and chloroaluminate ions exhibit similar binding energies and elemental signatures. To

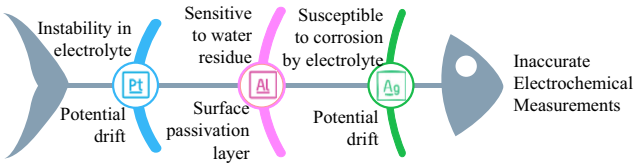

Figure 17. Fishbone diagram of pseudo-reference electrodes (Ag, Pt, Al wires).

address this ambiguity, complementary techniques capable of probing the bulk composition and structure of cathode materials are essential for discerning the true nature of Al species involved in the intercalation process.

6.5. Challenges with Detrimental Effects of Water in RABs

Water significantly impacts RABs due to its influence on the hydrogen evolution reaction (HER) and Al plating. Under standard conditions, the standard reduction potential (E^0) for HER (≈0 V vs standard hydrogen electrode (SHE)) is more favorable compared to Al reduction (≈−1.66 V vs SHE).[147] However, this thermodynamic driving force can still promote HER over Al plating even in nonstandard conditions. While HER may appear as a side reaction, it poses several challenges, including gas generation within the cell case and safety concerns. Additionally, it can interfere and compete with Al plating on the negative electrode surface. Even if Al can be plated successfully, the presence of water residue can lead to the formation of Al oxide/hydroxides, acting as nonconductive barriers that hinder further stripping processes and reduce plating and stripping efficiency. Furthermore, the HER reaction may alter the local pH, potentially causing electrolyte decomposition near the negative electrode.[148]

Unfortunately, the accurate determination and removal of water content from RAB electrolytes remain a challenge. For instance, tracking water in highly corrosive chloroaluminate IL-based electrolytes is difficult due to their corrosive nature, which could damage the Pt electrode used in Karl–Fischer titration or the SS of gas chromatograph coupled to a mass spectrometer (GC-MS). Despite employing high-purity precursors like $AlCl_3$ and EMImCl to minimize impurities, achieving absolute dryness after electrolyte preparation remains elusive.

In noncorrosive electrolytes, commercially available $Al(OTf)_3$ salts inherently contain water, as demonstrated by attenuated total reflectance–FTIR, Differential Scanning Calorimetry, and TGA–MS analyses. This bound water exhibits remarkable stability, resisting removal through thermal desorption or chemical dehydration. Heating $Al(OTf)_3$ beyond 200 °C likely leads to irreversible decomposition, forming an amorphous glass.[149]

Lastly, when tracking water content in electrolytes containing components like cyclic carbonates or additives (e.g., fluoroethylene carbonate, vinylene carbonate), specialized KF reagents are necessary. Any redox-active components, such as dimethyl sulfoxide (DMSO), can react with iodine in the reagent, potentially yielding false results.[150,151]

6.6. Challenges in Using Conventional Battery Laboratory Equipment for RAB Research

In RABs research, using conventional lab equipment poses several challenges due to the properties of the $AlCl_3$ salt and EMImCl. Both components are stored in a glove box. The electrolyte preparation involves the gradual addition of the $AlCl_3$ salt to the EMImCl, initially a powder, to obtain a yellowish-to-clear solution. As mentioned earlier, the process is exothermic, as indicated by vapor release during preparation. To mitigate issues related to electrolyte preparation, it is highly recommended to carefully control the amount of electrolyte prepared for experiments, we suggest maintaining it below 3 g of $AlCl_3$.

After preparation, the electrolyte should be covered with Al foil instead of a cap, as the vial cap would be destroyed by the continued vapor release. This results in an acidic environment in the glove box. The acidic nature of the electrolyte causes several issues. Corrosion is a primary concern, affecting the scale and the glove box pre-chambers as can be seen in **Figure 18**.

Cell holders connected to the potentiostat also corrode over time, necessitating regular replacement. Additionally, the glove box vacuum pump requires frequent servicing, depending on the activity in the glovebox or the number of experiments carried on in it, due to defects caused by acid vapors. Electrolyte leakage is another common problem, particularly with Swagelok cells, exacerbating the issue of equipment corrosion. These challenges highlight the need for specialized equipment and careful maintenance when conducting RABs research.

6.7. Waste Disposal Hazards and Environmental Concerns

After electrochemical testing, the electrolyte must be disposed of in special glass bottles, and the cells transported outside the glove box for cleaning. Exposure to air causes the remaining electrolyte to react, producing an abrasive vapor that poses a danger to researchers.

Additionally, proper management of hazardous waste is crucial for all cell components, including the metal anode, cathode material, separator, and current collector, all of which are soaked in electrolyte. These components require careful handling and disposal to mitigate environmental and health risks associated with their hazardous nature. This issue is not exclusive to RABs research but extends to other battery systems as well. For instance, in sodium-ion batteries, diglyme is often used as an electrolyte due to its comparable ionic conductivity to

Figure 18. Corroded SS glove box chamber.

carbonate-based electrolytes, satisfactory electrochemical stability across a wide voltage range, and potential to enhance battery performance.[152] However, diglyme is classified as a hazardous substance, with risks including flammability, toxicity, and potential harm to aquatic ecosystems, making its disposal particularly critical. This highlights the universal need for rigorous waste management practices across all battery technologies.

7. Summary and Outlook

This review highlights the significant advancements and challenges in the development of RABs.

So far, despite extensive research, the chloroaluminate IL-based electrolyte remains the most used one due to its efficiency in Al plating/stripping, although its corrosive nature poses substantial obstacles. Developing a noncorrosive electrolyte with high efficiency in Al plating/stripping could mitigate many issues, such as the stability of electrodes and current collectors. However, for the time being, the dissolution of electrode materials in the electrolyte and the instability of common binders and current collectors pose significant challenges.

Designing stable and high-capacity cathode materials for RABs is challenging, with each material class having its pros and cons. Carbon-based materials, particularly graphite, exhibit exceptional stability and cycling performance. In contrast, polymer-based materials, such as X-PVMPT, show outstanding electrochemical activity, exhibiting the same excellent stability as graphite while delivering superior specific capacity, but often requiring conductivity enhancement strategies. Transition metal oxides and chalcogenides, in contrast, face significant degradation, primarily due to dissolution during cycling. MXenes, especially in their delaminated form, demonstrate high specific capacities and excellent stability, but their efficiency is often limited by irreversible interactions with intercalating ions and surface termination groups. To address the dissolution of transition metal oxides and chalcogenides, heterostructures have been developed to mitigate capacity loss by preventing the dissolution of active materials.

Regarding binders, common ones like PVdF and CMC react with the chloroaluminate IL-based electrolyte. Therefore, using stable polymers such as PTFE and polyimide as binders is highly recommended. Additionally, employing corrosion-resistant current collectors like TiN, Cr_2N, or ITO, instead of metals like Al, Au, Cu, Mo, Ni, and Pt, can enhance the performance, longevity of RABs as well as ensure reliable performance assessments and prevent misleading results caused by side reactions or degradation.

In addition to the limitations posed by the stability of materials used in RABs within the corrosive chloroaluminate IL-based electrolyte, technical challenges, especially those related to these corrosive electrolytes, have hindered the application of advanced analysis techniques necessary for understanding charge/discharge mechanisms. To date, specialized cell designs capable of withstanding harsh conditions are crucial for real-time observation and analysis, which would greatly benefit the RAB research community. This is an open invitation for researchers and engineers to explore deeper into solving these.

Overall, addressing the issues mentioned in this review may pave the way to achieving the high theoretical volumetric capacity promised by RABs, while also making them safe enough for practical applications.

Acknowledgements

The authors acknowledge Dr. Angelina Sarapulova for her invaluable contributions to all the experiments conducted, which were essential for the knowledge presented here. The authors also appreciate Dr. Nicholas Jobbitt's help in refining the language. Additionally, the authors extend their thanks to the assistance of Copilot AI in enhancing the clarity and transparency of the text as well as to Slidesgo for providing some of the figure design templates. This work contributes to the research performed at CELEST (Center for Electrochemical Energy Storage Ulm-Karlsruhe) and was funded by the German Research Foundation (DFG) under Project ID 390874152 (POLiS Cluster of Excellence).

Open Access funding enabled and organized by Projekt DEAL.

Conflict of Interest

The authors declare no conflict of interest.

Author Contributions

The authors contributed to this work as follows: **Mahla Talari** focused on the electrolyte, **Eliana Fuentes-Mendoza** and **Rafael Cordoba** worked on the positive electrode, and **Eugen Zemlyanushin** handled the negative electrode, current collector, and binders. **Sonia Dsoke** supervised the overall work. The technical challenges were addressed collaboratively by all authors, based on individual experience. All authors contributed to conceiving the review, writing, and editing.

Keywords: aluminum batteries · challenges · ionic liquid electrolytes · post-lithium

[1] European Union (EU), Long-Term Low Greenhouse Gas Emission Development Strategies **2020**.
[2] Y. Wu, W. Shuang, Y. Wang, F. Chen, S. Tang, X. L. Wu, Z. Bai, L. Yang, J. Zhang, *Electrochem. Energy Rev.* **2024**, *7*, 17.
[3] M. R. Palacin, P. Johansson, R. Dominko, B. Dlugatch, D. Aurbach, Z. Li, M. Fichtner, O. Lužanin, J. Bitenc, Z. Wei, C. Glaser, J. Janek, A. Fernández-Barquín, A. R. Mainar, O. Leonet, I. Urdampilleta, J. A. Blázquez, D. S. Tchitchekova, A. Ponrouch, P. Canepa, G. S. Gautam, R. S. R. G. Casilda, C. S. Martinez-Cisneros, N. U. Torres, A. Varez, J. Y. Sanchez, K. V. Kravchyk, M. V. Kovalenko, A. A. Teck, H. Shiel, et al., *J. Phys. Energy* **2024**, *6*, 031501.
[4] X. Xu, K. S. Hui, K. N. Hui, J. Shen, G. Zhou, J. Liu, Y. Sun, *J. Chem. Eng.* **2021**, *418*, 129385.
[5] D. E. Couch, A. Brenner, *J. Electrochem. Soc.* **1952**, *99*, 234.
[6] N. Ishibashi, M. Yoshio, *Electrochim. Acta* **1972**, *17*, 1343.
[7] W. A. Badawy, B. A. Sabrah, N. H. Y. Hilal, *J. Appl. Electrochem.* **1987**, *17*, 357.
[8] T. Yao, H. Yang, K. Wang, W. Wu, H. Jiang, H. Liu, Q. Wang, W. Ding, *Materials* **2020**, *13*, 5506.

[9] G. L. Holleck, J. Giner, B. Burrows, *Rechageable Conf. Proc.*, Seattle, USA **1972**.
[10] M. Jafarian, M. G. Mahjani, F. Gobal, I. Danaee, *J. Appl. Electrochem.* **2006**, *36*, 1169.
[11] J. Wang, X. Zhang, W. Chu, S. Liu, H. Yu, *Chem. Commun.* **2019**, *55*, 2138.
[12] N. Jayaprakash, S. K. Das, L. A. Archer, *Chem. Commun.* **2011**, *47*, 12610.
[13] M. L. Agiorgousis, Y.-Y. Sun, S. Zhang, *ACS Energy Lett.* **2017**, *2*, 689.
[14] M. Angell, C.-J. Pan, Y. Rong, C. Yuan, M.-C. Lin, B.-J. Hwang, H. Dai, *Proc. Natl. Acad. Sci.* **2017**, *114*, 834.
[15] T. C. Huynh, Q. P. D. Dao, T.-N. Truong, N.-G. Doan, S.-L. Ho, *Environ. Pollut.* **2014**, *3*, 59.
[16] D. Yuan, J. Zhao, W. Manalastas, S. Kumar, M. Srinivasan, *Nano Mater. Sci.* **2020**, *2*, 248.
[17] M. Galiński, A. Lewandowski, I. Stępniak, *Electrochim. Acta* **2006**, *51*, 5567.
[18] X. Han, Y. Bai, R. Zhao, Y. Li, F. Wu, C. Wu, *Prog. Mater. Sci.* **2022**, *128*, 100960.
[19] D. Ma, D. Yuan, C. Ponce de León, Z. Jiang, X. Xia, J. Pan, *Energy Environ. Mater.* **2022**, *6*, e12301.
[20] G. A. Giffin, *J. Mater. Chem. A* **2016**, *4*, 13378.
[21] Y. Zhao, T. J. VanderNoot, *Electrochim. Acta* **1997**, *42*, 3.
[22] P. Wasserscheid, T. Welton, *Ionic Liquids in Synthesis*, Wiley-VCH Verlag GmbH & Co. KGaA, Weinheim, Germany **2002**.
[23] D. Muñoz-Torrero, J. Palma, R. Marcilla, E. Ventosa, *Dalton Trans.* **2019**, *48*, 9906.
[24] H. Wang, S. Gu, Y. Bai, S. Chen, N. Zhu, C. Wu, F. Wu, *J. Mater. Chem. A* **2015**, *3*, 22677.
[25] K. L. Ng, Z. Lu, Y. Wang, C. V. Singh, G. Azimi, *J. Phys. Chem. C* **2021**, *125*, 15145.
[26] G. F. Reynolds, C. J. Dymek, *J. Power Sources* **1985**, *15*, 109.
[27] S. Zein El Abedin, P. Giridhar, P. Schwab, F. Endres, *Electrochem. Commun.* **2010**, *12*, 1084.
[28] H. Yang, F. Wu, Y. Bai, C. Wu, *J. Energy Chem.* **2020**, *45*, 98.
[29] Z. Hu, H. Zhang, H. Wang, F. Zhang, Q. Li, H. Li, *ACS Mater. Lett.* **2020**, *2*, 887.
[30] Q.-X. Qin, M. Skyllas-Kazacos, *J. Electroanal. Chem. Interface Electrochem.* **1984**, *168*, 193.
[31] H. Kan, Z. Wang, X. Wang, N. Zhang, *Trans. Nonferrous Met. Soc. China* **2010**, *20*, 158.
[32] V. A. Elterman, P. Y. Shevelin, L. A. Yolshina, E. G. Vovkotrub, A. V. Borozdin, *J. Mol. Liq.* **2020**, *320*, 114482.
[33] R. T. Carlin, R. A. Osteryoung, *J. Electrochem. Soc.* **1989**, *136*, 1409.
[34] T. J. Melton, J. Joyce, J. T. Maloy, J. A. Boon, J. S. Wilkes, *J. Electrochem. Soc.* **1990**, *137*, 3865.
[35] Y. Chryssoulakis, J.-C. Poignet, G. Manoli, *J. Appl. Electrochem.* **1987**, *17*, 857.
[36] S. Wang, K. V. Kravchyk, F. Krumeich, M. V. Kovalenko, *ACS Appl. Mater. Interfaces* **2017**, *9*, 28478.
[37] Y. Oh, G. Lee, Y. Tak, *ChemElectroChem* **2018**, *5*, 3348.
[38] Y. Zhang, S. Liu, Y. Ji, J. Ma, H. Yu, *Adv. Mater.* **2018**, *30*, 1870063.
[39] X. Wu, N. Qin, F. Wang, Z. Li, J. Qin, G. Huang, D. Wang, P. Liu, Q. Yao, Z. Lu, J. Deng, *Energy Storage Mater.* **2021**, *37*, 619.
[40] K. Yoshida, M. Nakamura, Y. Kazue, N. Tachikawa, S. Tsuzuki, S. Seki, K. Dokko, M. Watanabe, *J. Am. Chem. Soc.* **2011**, *133*, 13121.
[41] S. Terada, T. Mandai, R. Nozawa, K. Yoshida, K. Ueno, S. Tsuzuki, K. Dokko, M. Watanabe, *Phys. Chem. Chem. Phys.* **2014**, *16*, 11737.
[42] C. Xu, T. Diemant, A. Mariani, M. E. Di Pietro, A. Mele, X. Liu, S. Passerini, *Angew. Chem. Int. Ed.* **2024**, *63*, e202318204.
[43] M. W. M. Graef, *J. Electrochem. Soc.* **1985**, *132*, 1038.
[44] M. C. Lefebvre, B. E. Conway, *J. Electroanal. Chem.* **2000**, *480*, 34.
[45] M. C. Lefebvre, B. E. Conway, *J. Electroanal. Chem.* **2000**, *480*, 46.
[46] M. Yoshio, N. Ishibashi, *J. Appl. Electrochem.* **1973**, *3*, 321.
[47] X. Wen, Y. Liu, D. Xu, Y. Zhao, R. K. Lake, J. Guo, *J. Phys. Chem. Lett.* **2020**, *11*, 1589.
[48] M. Miyake, H. Fujii, T. Hirato, *Surf. Coat. Technol.* **2015**, *277*, 160.
[49] L. Legrand, A. Tranchant, R. Messina, *J. Electrochem. Soc.* **1994**, *141*, 378.
[50] Y. Nakayama, Y. Senda, H. Kawasaki, N. Koshitani, S. Hosoi, Y. Kudo, H. Morioka, M. Nagamine, *Phys. Chem. Chem. Phys.* **2015**, *17*, 5758.
[51] L. Legrand, M. Heintz, A. Tranchant, R. Messina, *Electrochim. Acta* **1995**, *40*, 1711.
[52] Z. Zhang, A. Kitada, S. Gao, K. Fukami, N. Tsuji, Z. Yao, K. Murase, *ACS Appl. Mater. Interfaces* **2020**, *12*, 43289.
[53] M. Li, B. Gao, C. Liu, W. Chen, Z. Shi, X. Hu, Z. Wang, *Electrochim. Acta* **2015**, *180*, 811.
[54] T. Mandai, P. Johansson, *J. Phys. Chem. C* **2016**, *120*, 21285.
[55] H. Yang, H. Li, J. Li, Z. Sun, K. He, H. Cheng, F. Li, *Angew. Chem. Int. Ed.* **2019**, *58*, 11978.
[56] X. Zhang, T. M. Devine, *J. Electrochem. Soc.* **2006**, *153*, B375.
[57] I. N. Pyagai, L. A. Pasechnik, A. S. Yatsenko, V. M. Skachkov, S. P. Yatsenko, *Russ. J. Appl. Chem.* **2012**, *85*, 1649.
[58] Q. Li, J. O. Jensen, N. J. Bjerrum, *Encyclopedia of Electrochemical Power Sources* **2009**, pp. 695–708.
[59] H. Wang, D. Y. C. Leung, M. K. H. Leung, *Appl. Energy* **2012**, *90*, 100.
[60] S. Yang, H. Knickle, *J. Power Sources* **2002**, *112*, 162.
[61] IAI, Global Aluminium Recycling: A Cornerstone of Sustainable Development **2009**, https://international-aluminium.org/wp-content/uploads/2009/06/Global-aluminium-recycling.pdf, (accessed: August 2024).
[62] T. Leisegang, F. Meutzner, M. Zschornak, W. Münchgesang, R. Schmid, T. Nestler, R. A. Eremin, A. A. Kabanov, V. A. Blatov, D. C. Meyer, *Front. Chem.* **2019**, *7*, 268.
[63] N. Sabi, K. Palanisamy, F. Rahide, S. Daboss, C. Kranz, S. Dsoke, *Batteries Supercaps* **2023**, *6*, e202300298.
[64] M. Textor, M. Amstutz, *Anal. Chim. Acta* **1994**, *297*, 15.
[65] D. Lee, G. Lee, Y. Tak, *Nanotechnology* **2018**, *29*, 36LT01.
[66] M. Jiang, C. Fu, P. Meng, J. Ren, J. Wang, J. Bu, A. Dong, J. Zhang, W. Xiao, B. Sun, *Adv. Mater.* **2021**, *34*, 2102026.
[67] Y. Gu, Y. Liu, Y. Tong, Z. Qin, Z. Wu, W. Hu, *Nanomaterials* **2022**, *12*, 1336.
[68] S. Choi, H. Go, G. Lee, Y. Tak, *Phys. Chem. Chem. Phys.* **2017**, *19*, 8653.
[69] J. Shi, J. Zhang, J. Guo, *ACS Energy Lett.* **2019**, *4*, 2124.
[70] M. Wang, F. Zhang, C. Lee, Y. Tang, *Adv. Energy Mater.* **2017**, *7*, 1700536.
[71] S. K. Das, S. Mahapatra, H. Lahan, *J. Mater. Chem. A* **2017**, *5*, 6347.
[72] G. Razaz, S. Arshadirastabi, N. Blomquist, J. Örtegren, T. Carlberg, M. Hummelgård, H. Olin, *Materials* **2023**, *16*, 933.
[73] S. Chowdhury, N. Sabi, R. C. Rojano, N. Le Breton, A. K. Boudalis, S. Klayatskaya, S. Dsoke, M. Ruben, *Batteries Supercaps* **2024**, *7*, e202300285.
[74] B. Craig, T. Schoetz, A. Cruden, C. Ponce de Leon, *Renewable Sustainable Energy Rev.* **2020**, *133*, 110100.
[75] K. Zhang, T. H. Lee, J. H. Cha, H. W. Jang, J. W. Choi, M. Mahmoudi, M. Shokouhimehr, *Sci. Rep.* **2019**, *9*, 13739.
[76] Z. Li, L. Y. Zhang, L. Zhang, J. Huang, H. Liu, *Nanoscale Res. Lett.* **2019**, *14*, 358.
[77] W. Xing, D. Du, T. Cai, X. Li, J. Zhou, Y. Chai, Q. Xue, Z. Yan, *J. Power Sources* **2018**, *401*, 6.
[78] Z. Huang, X. Du, M. Ma, S. Wang, Y. Xie, Y. Meng, W. You, L. Xiong, *ChemSusChem* **2023**, *16*, e202202358.
[79] M. P. Paranthaman, G. Brown, X.-G. Sun, J. Nanda, A. Manthiram, A. Manivannan, in *ECS Meeting Abstracts*, Vancouver, Canada **2010**.
[80] H. Wang, Y. Bai, S. Chen, X. Luo, C. Wu, F. Wu, J. Lu, K. Amine, *ACS Appl. Mater. Interfaces* **2014**, *7*, 80.
[81] J. Liu, Z. Li, X. Huo, J. Li, *J. Power Sources* **2019**, *422*, 49.
[82] X. Zhang, G. Zhang, S. Wang, S. Li, S. Jiao, *J. Mater. Chem. A* **2018**, *6*, 3084.
[83] N. Zhu, F. Wu, Z. Wang, L. Ling, H. Yang, Y. Gao, S. Guo, L. Suo, H. Li, H. Xu, Y. Bai, C. Wu, *J. Energy Chem.* **2020**, *51*, 72.
[84] J. Wei, W. Chen, D. Chen, K. Yang, *J. Electrochem. Soc.* **2017**, *164*, A2304.
[85] S. Nandi, M. Pumera, *ChemSusChem* **2024**, *17*, e202301434.
[86] Z. Li, B. Niu, J. Liu, J. Li, F. Kang, *ACS Appl. Mater. Interfaces* **2018**, *10*, 9451.
[87] Z. Zhao, Z. Hu, H. Liang, S. Li, H. Wang, F. Gao, X. Sang, H. Li, *ACS Appl. Mater. Interfaces* **2019**, *11*, 44333.
[88] C. G. Hawkins, A. Verma, W. Horbinski, R. Weeks, P. P. Mukherjee, L. Whittaker-Brooks, *ACS Appl. Mater. Interfaces* **2020**, *12*, 21788.
[89] H. Lei, M. Wang, J. Tu, S. Jiao, *Sustainable Energy Fuels* **2019**, *3*, 2717.
[90] Z. Yu, S. Jiao, J. Tu, Y. Luo, W.-L. Song, H. Jiao, M. Wang, H. Chen, D. Fang, *ACS Nano* **2020**, *14*, 3469.
[91] C. Zheng, J. Tu, S. Jiao, M. Wang, Z. Wang, *ACS Appl. Energy Mater.* **2020**, *3*, 12635.
[92] J. Wu, D. Wu, M. Zhao, Z. Wen, J. Jiang, J. Zeng, J. Zhao, *Dalton Trans.* **2020**, *49*, 729.
[93] X. Yu, A. Manthiram, *Adv. Energy Mater.* **2017**, *7*, 1700561.
[94] H. Lei, J. Tu, W.-L. Song, H. Jiao, X. Xiao, S. Jiao, *Inorg. Chem. Front.* **2021**, *8*, 1030.
[95] X. Zhang, S. Jiao, J. Tu, W.-L. Song, X. Xiao, S. Li, M. Wang, H. Lei, D. Tian, H. Chen, D. Fang, *Energy Environ. Sci.* **2019**, *12*, 1918.
[96] L. Chai, X. Li, W. Lv, G. Wu, W. Zhang, Z. Li, *ACS Appl. Mater. Interfaces* **2022**, *14*, 48780.
[97] H. Yang, L. Yin, J. Liang, Z. Sun, Y. Wang, H. Li, K. He, L. Ma, Z. Peng, S. Qiu, C. Sun, H. M. Cheng, F. Li, *Angew. Chem. Int. Ed.* **2018**, *57*, 1898.
[98] T. Zhang, T. Cai, W. Xing, T. Li, B. Liang, H. Hu, L. Zhao, X. Li, Z. Yan, *Energy Storage Mater.* **2021**, *41*, 667.

[99] H. Jiao, D. Tian, S. Li, C. Fu, S. Jiao, *ACS Appl. Energy Mater.* **2018**, *1*, 4924.
[100] H. Li, R. Meng, Y. Guo, B. Chen, Y. Jiao, C. Ye, Y. Long, A. Tadich, Q. H. Yang, M. Jaroniec, S. Z. Qiao, *Nat. Commun.* **2021**, *12*, 5714.
[101] X. Yang, C. Huang, *J. Energy Storage* **2024**, *78*, 110069.
[102] M.-C. Lin, M. Gong, B. Lu, Y. Wu, D.-Y. Wang, M. Guan, M. Angell, C. Chen, J. Yang, B.-J. Hwang, H. Dai, *Nature* **2015**, *520*, 324.
[103] J. Qiao, H. Zhou, Z. Liu, H. Wen, J. Du, G. Wei, C. He, J. Yang, *Ionics* **2019**, *26*, 245.
[104] H. Jiao, J. Wang, J. Tu, H. Lei, S. Jiao, *Energy Technol.* **2016**, *4*, 1112.
[105] S. Divya, T. Nann, *ChemElectroChem* **2020**, *8*, 492.
[106] C. Huang, Y. Yang, M. Li, X. Qi, C. Pan, K. Guo, L. Bao, X. Lu, *Adv. Mater.* **2023**, *36*, 2306244.
[107] N. S. Hudak, *J. Phys. Chem. C* **2014**, *118*, 5203.
[108] M. Walter, K. V. Kravchyk, C. Böfer, R. Widmer, M. V. Kovalenko, *Adv. Mater.* **2018**, *30*, 1705644.
[109] G. Studer, A. Schmidt, J. Büttner, M. Schmidt, A. Fischer, I. Krossing, B. Esser, *Energy Environ. Sci.* **2023**, *16*, 3760.
[110] C. Wang, Z. Pan, H. Chen, X. Pu, Z. Chen, *Batteries* **2023**, *9*, 174.
[111] X. Huo, X. Wang, Z. Li, J. Liu, J. Li, *Nanoscale* **2020**, *12*, 3387.
[112] A. VahidMohammadi, A. Hadjikhani, S. Shahbazmohamadi, M. Beidaghi, *ACS Nano* **2017**, *11*, 11135.
[113] L. Yao, S. Ju, X. Yu, *J. Mater. Chem. A* **2021**, *9*, 16878.
[114] R. Zhuang, Z. Huang, S. Wang, J. Qiao, J. C. Wu, J. Yang, *J. Chem. Eng.* **2021**, *409*, 128235.
[115] T. Cai, L. Zhao, H. Hu, T. Li, X. Li, S. Guo, Y. Li, Q. Xue, W. Xing, Z. Yan, L. Wang, *Energy Environ. Sci.* **2018**, *11*, 2341.
[116] J. Li, L. Kang, K. Luo, Y. Huang, S. Zhong, D. Yan, *Ceram. Int.* **2023**, *49*, 2613.
[117] L. Chen, W. Song, N. Li, H. Jiao, X. Han, Y. Luo, M. Wang, H. Chen, S. Jiao, D. Fang, *Adv. Mater.* **2020**, *32*, 2001212.
[118] P. Saxena, P. Shukla, *Adv. Compos. Hybrid Mater.* **2021**, *4*, 8.
[119] W. Zhou, Y. Lin, K. Zou, C. Zhou, X. Gong, Y. Cao, S. Jiang, *J. Mater. Sci.: Mater. Electron.* **2021**, *32*, 28708.
[120] Y. Uemura, C.-Y. Chen, Y. Hashimoto, T. Tsuda, H. Matsumoto, S. Kuwabata, *ACS Appl. Energy Mater.* **2018**, *1*, 2269.
[121] J. Smajic, A. Alazmi, P. M. F. J. Costa, *MRS Adv.* **2019**, *4*, 807.
[122] L.-L. Chen, N. Li, H. Shi, Y. Zhang, W.-L. Song, S. Jiao, H. Chen, D. Fang, *Nano Res.* **2020**, *13*, 419.
[123] J. Yu, X. Li, N. Li, T. Wu, Y. Liu, C. Li, J. Liu, L. Wang, *Small Methods* **2022**, *6*, 2200026.
[124] Z. Yu, Y. Xie, W. Wang, J. Hong, J. Ge, *Front. Chem.* **2023**, *11*, 1190102.
[125] Z. Yang, M. Guo, P. Meng, M. Jiang, X. Qiu, J. Zhang, C. Fu, *Chem. – Eur. J.* **2023**, *29*, 2203546.
[126] E. Zemlyanushin, A. L. Müller, T. Tsuda, S. Dsoke, *J. Electrochem. Soc.* **2024**, *171*, 110507.
[127] K. Matsumoto, D. Minori, K. Takagi, R. Hagiwara, *Carbon* **2014**, *67*, 434.
[128] Q. Wang, D. Zheng, L. He, X. Ren, *Phys. Rev. Appl.* **2019**, *12*, 072013.
[129] S. Hina, Y. Zhang, H. Wang, *Rev. Adv. Mater. Sci.* **2015**, *40*, 215.
[130] A. Marzec, A. Laskowska, G. Boiteux, M. Zaborski, O. Gain, A. Serghei, *Macromol. Symp.* **2014**, *341*, 7.
[131] M.-C. Huang, C.-H. Yang, C.-C. Chiang, S.-C. Chiu, Y.-F. Chen, C.-Y. Lin, L.-Y. Wang, Y.-L. Li, C.-C. Yang, W.-S. Chang, *Energies* **2018**, *11*, 2760.
[132] W. A. Appiah, M. P. Stockham, J. M. Garcia Lastra, *Batteries Supercaps* **2023**, *6*, e202300258.
[133] Q. Zhao, M. J. Zachman, W. I. Al Sadat, J. Zheng, L. F. Kourkoutis, L. Archer, *Sci. Adv.* **2018**, *4*, eaau8131.
[134] T. Dong, K. L. Ng, Y. Wang, O. Voznyy, G. Azimi, *Adv. Energy Mater.* **2021**, *11*, 2100077.
[135] B. Zhang, W. Zhang, H. Jin, J. Wan, *ChemistrySelect* **2023**, *8*, 2204575.
[136] S. Wang, K. V. Kravchyk, A. N. Filippin, U. Müller, A. N. Tiwari, S. Buecheler, M. I. Bodnarchuk, M. V. Kovalenko, *Adv. Sci.* **2018**, *5*, 1700712.
[137] TSC 1600 Closed - rhd instruments, https://rhd-instruments.de/en/products/cells/tsc-1600-closed (accessed: August 2024).
[138] rhd-instruments, Instruments, TSC Battery - rhd, https://rhd-instruments.de/en/products/cells/tsc-battery (accessed: August 2024).
[139] TSC Surface - rhd instruments, https://rhd-instruments.de/en/products/cells/tsc-surface (accessed: August 2024).
[140] E. Zemlyanushin, B. Schwarz, S. Dsoke, *J. Power Sources* **2025**, *633*, 236458.
[141] Y. Yi, G. Weinberg, M. Prenzel, M. Greiner, S. Heumann, S. Becker, R. Schlögl, *Catal. Today* **2017**, *295*, 32.
[142] S. J. Teh, C. W. Lai, *Applications of Nanocomposite Materials in Dentistry*, Elsevier, Amsterdam, Netherlands **2019**, pp. 93–105.
[143] S. Sharma, *Materials* **2018**, *11*, 1857.
[144] P. W. Ruch, D. Cericola, M. Hahn, R. Kötz, A. Wokaun, *J. Electroanal. Chem.* **2009**, *636*, 128.
[145] S. E. Lee, M. H. Tang, *J. Electrochem. Soc.* **2019**, *166*, A3260.
[146] K. Pfeifer, S. Arnold, J. Becherer, C. Das, J. Maibach, H. Ehrenberg, S. Dsoke, *ChemSusChem* **2019**, *12*, 3312.
[147] D. R. Lide, *CRC Handbook of Chemistry and Physics*, CRC Press, Boca Raton, FL, USA **2004**.
[148] M. Talari, A. Sarapulova, E. Zemlyanushin, N. Sabi, A. Hofmann, V. Trouillet, S. Dsoke, *Batteries Supercaps* **2024**, *8*, e202400317.
[149] G. R. Pastel, Y. Chen, T. P. Pollard, M. A. Schroeder, M. E. Bowden, A. Zheng, N. T. Hahn, L. Ma, V. Murugesan, J. Ho, *Energy Environ. Sci.* **2022**, *15*, 2460.
[150] Sigma-Aldrich, Accurate Water Determination Aquastar Karl Fischer **2024**, https://www.sigmaaldrich.com/deepweb/assets/sigmaaldrich/marketing/global/documents/128/403/aquastar-reagents-br3083en-mk.pdf (accessed: August 2024).
[151] Honeywell International Inc., Accurate Water Determination in Lithium-Ion Batteries with HydranalTM Nextgen Coulomat A-Fa And C-Fa **2018**, https://lab.honeywell.com/content/dam/rc/en/resources/resource-library/articles-and-whitepapers/accurate-water-determination-in-lithium-ion-batteries-with-hydranal-nextgen-coulomat-a-fa-and-c-fa.pdf (accessed: August 2024).
[152] K. Westman, R. Dugas, P. Jankowski, W. Wieczorek, G. Gachot, M. Morcrette, E. Irisarri, A. Ponrouch, M. R. Palacín, J. M. Tarascon, P. Johansson, *ACS Appl. Energy Mater.* **2018**, *1*, 2671.
[153] L. D. Reed, A. Arteaga, E. J. Menke, *J. Phys. Chem. B* **2015**, *119*, 12677.
[154] L. D. Reed, S. N. Ortiz, M. Xiong, E. J. Menke, *Chem. Commun.* **2015**, *51*, 14397.
[155] T. Mandai, P. Johansson, *J. Mater. Chem. A* **2015**, *3*, 12230.
[156] U. S. Department of Energy, Energy Requirements for Aluminum Production: Historical Perspective. Theoretical Limits and Current Practices **2007**, https://www1.eere.energy.gov/manufacturing/resources/aluminum/pdfs/al_theoretical.pdf (accessed: September 2024).
[157] H. Chen, H. Xu, B. Zheng, S. Wang, T. Huang, F. Guo, W. Gao, C. Gao, *ACS Appl. Mater. Interfaces* **2017**, *9*, 22628.
[158] M. Chiku, S. Matsumura, H. Takeda, E. Higuchi, H. Inoue, *J. Electrochem. Soc.* **2017**, *164*, A1841.
[159] X. Wen, J. Zhang, H. Luo, J. Shi, C. Tsay, H. Jiang, Y.-H. Lin, M. A. Schroeder, K. Xu, J. Guo, *J. Phys. Chem. Lett.* **2021**, *12*, 5903.
[160] Z. Slim, E. J. Menke, *J. Phys. Chem. B* **2020**, *124*, 5002.
[161] Z. Slim, E. J. Menke, *J. Phys. Chem. C* **2022**, *126*, 2365.
[162] Z. Slim, E. J. Menke, *Batteries Supercaps* **2023**, *6*, e202300164.
[163] J. Bitenc, N. Lindahl, A. Vizintin, M. E. Abdelhamid, R. Dominko, P. Johansson, *Energy Storage Mater.* **2020**, *24*, 379.
[164] D. J. Kim, D.-J. Yoo, M. T. Otley, A. Prokofjevs, C. Pezzato, M. Owczarek, S. J. Lee, J. W. Choi, J. F. Stoddart, *Nat. Energy* **2018**, *4*, 51.
[165] J. Tu, M. Wang, Y. Luo, S. Jiao, *ACS Sustainable Chem. Eng.* **2020**, *8*, 2416.
[166] S. Liu, J. J. Hu, N. F. Yan, G. L. Pan, G. R. Li, X. P. Gao, *Energy Environ. Sci.* **2012**, *5*, 9743.
[167] Z. Li, X. Wang, W. Zhang, S. Yang, *J. Chem. Eng.* **2020**, *398*, 125679.
[168] X. Wang, R. Zhuang, X. Liu, M. Hu, P. Shen, J. Luo, J. Yang, J. Wu, *Nanomaterials* **2024**, *14*, 442.
[169] S. Lu, T. Lu, W. Luo, Z. Chao, Y. Liu, Z. Zhang, J. Fan, *Energy Fuels* **2022**, *36*, 7890.
[170] B. Tan, S. Han, W. Luo, Z. Chao, J. Fan, M. Wang, *J. Alloys Compd.* **2020**, *841*, 155732.

Manuscript received: December 23, 2024
Revised manuscript received: March 12, 2025
Version of record online: April 8, 2025